Journal of Instrumentation

The electromagnetic calorimeter for the T2K near detector ND280

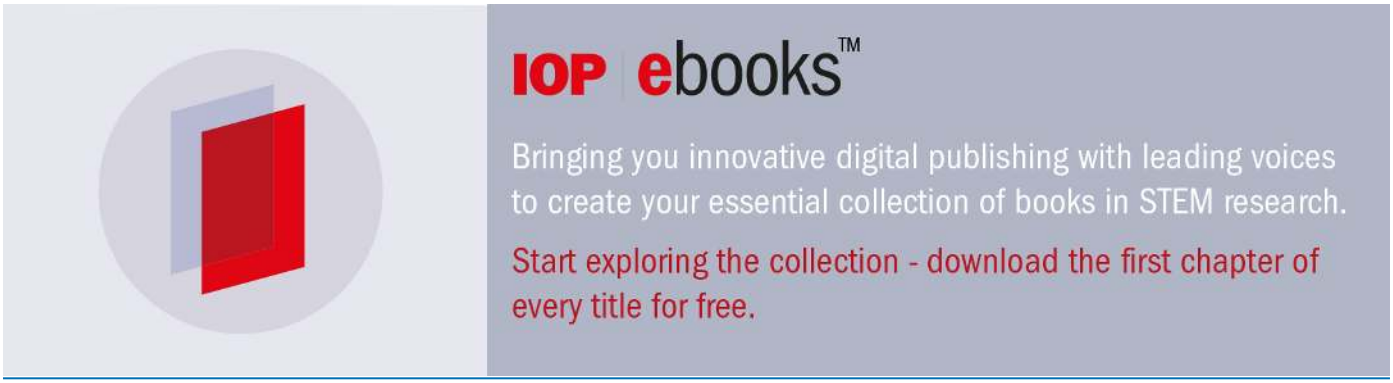

PUBLISHED BY IOP PUBLISHING FOR SISSA MEDIALAB

RECEIVED: *August 15, 2013*
ACCEPTED: *September 4, 2013*
PUBLISHED: *October 17, 2013*

The electromagnetic calorimeter for the T2K near detector ND280

The T2K UK collaboration

D. Allan,[e] C. Andreopoulos,[e] C. Angelsen,[e] G.J. Barker,[i] G. Barr,[g] S. Bentham,[c] I. Bertram,[c] S. Boyd,[i] K. Briggs,[i] R.G. Calland,[f] J. Carroll,[f] S.L. Cartwright,[h] A. Carver,[i] C. Chavez,[f] G. Christodoulou,[f] J. Coleman,[f] P. Cooke,[f] G. Davies,[c] C. Densham,[e] F.Di Lodovico,[d] J. Dobson,[b] T. Duboyski,[d] T. Durkin,[e] D.L. Evans,[f] A. Finch,[c] M. Fitton,[e] F.C. Gannaway,[d] A. Grant,[a] N. Grant,[c] S. Grenwood,[b] P. Guzowski,[b] D. Hadley,[i] M. Haigh,[g] P.F. Harrison,[i] A. Hatzikoutelis,[c] T.D.J. Haycock,[h] A. Hyndman,[d] J. Ilic,[e] S. Ives,[b] A.C. Kaboth,[b] V. Kasey,[b] L. Kellet,[f] M. Khaleeq,[b] G. Kogan,[b] L.L. Kormos,[c,1] M. Lawe,[h] T.B. Lawson,[h] C. Lister,[i] R.P. Litchfield,[i] M. Lockwood,[f] M. Malek,[b] T. Maryon,[c] P. Masliah,[b] K. Mavrokoridis,[f] N. McCauley,[f] I. Mercer,[c] C. Metelko,[e] B. Morgan,[i] J. Morris,[d] A. Muir,[a] M. Murdoch,[f] T. Nicholls,[e] M. Noy,[b] H.M. O'Keeffe,[g] R.A. Owen,[d] D. Payne,[f] G.F. Pearce,[e] J.D. Perkin,[h] E. Poplawska,[d] R. Preece,[e] W. Qian,[e] P. Ratoff,[c] T. Raufer,[e] M. Raymond,[b] M. Reeves,[c] D. Richards,[i] M. Rooney,[e] R. Sacco,[d] S. Sadler,[h] P. Schaack,[b] M. Scott,[b] D.I. Scully,[i] S. Short,[b] M. Siyad,[e] R. Smith,[g] B. Still,[d] P. Sutcliffe,[f] I.J. Taylor,[i] R. Terri,[d] L.F. Thompson,[h] A. Thorley,[f] M. Thorpe,[e] C. Timis,[d] C. Touramanis,[f] M.A. Uchida,[d] Y. Uchida,[b] A. Vacheret,[g] J.F. Van Schalkwyk,[b] O. Veledar,[h] A.V. Waldron,[g] M.A. Ward,[h] G.P. Ward,[h] D. Wark,[e,g] M.O. Wascko,[b] A. Weber,[e,g] N. West,[g] L.H. Whitehead,[i] C. Wilkinson[h] and J.R. Wilson[d]

[a] *STFC, Daresbury Laboratory, Daresbury, U.K.*
[b] *Imperial College London, London, U.K.*
[c] *Lancaster University, Lancaster, U.K.*
[d] *Queen Mary, University of London, London, U.K.*
[e] *STFC, Rutherford Appleton Laboratory, Oxford, U.K.*
[f] *University of Liverpool, Liverpool, U.K.*
[g] *University of Oxford, Oxford, U.K.*
[h] *University of Sheffield, Sheffield, U.K.*
[i] *University of Warwick, Coventry, U.K.*

E-mail: l.kormos@lancaster.ac.uk

[1] Corresponding author.

doi:10.1088/1748-0221/8/10/P10019

2013 JINST 8 P10019

ABSTRACT: The T2K experiment studies oscillations of an off-axis muon neutrino beam between the J-PARC accelerator complex and the Super-Kamiokande detector. Special emphasis is placed on measuring the mixing angle θ_{13} by observing ν_e appearance via the sub-dominant $\nu_\mu \rightarrow \nu_e$ oscillation and searching for CP violation in the lepton sector. The experiment includes a sophisticated, off-axis, near detector, the ND280, situated 280 m downstream of the neutrino production target in order to measure the properties of the neutrino beam and to understand better neutrino interactions at the energy scale below a few GeV. The data collected with the ND280 are used to study charged- and neutral-current neutrino interaction rates and kinematics prior to oscillation, in order to reduce uncertainties in the oscillation measurements by the far detector. A key element of the near detector is the ND280 electromagnetic calorimeter (ECal), consisting of active scintillator bars sandwiched between lead sheets and read out with multi-pixel photon counters (MPPCs). The ECal is vital to the reconstruction of neutral particles, and the identification of charged particle species. The ECal surrounds the Pi-0 detector (PØD) and the tracking region of the ND280, and is enclosed in the former UA1/NOMAD dipole magnet. This paper describes the design, construction and assembly of the ECal, as well as the materials from which it is composed. The electronic and data acquisition (DAQ) systems are discussed, and performance of the ECal modules, as deduced from measurements with particle beams, cosmic rays, the calibration system, and T2K data, is described.

KEYWORDS: Calorimeters; Neutrino detectors; Scintillators and scintillating fibres and light guides

ARXIV EPRINT: 1308.3445

2013 JINST 8 P10019

Contents

2013 JINST 8 P10019

1 Introduction

Many parameters of neutrino oscillations have yet to be measured precisely. The Tokai-to-Kamioka (T2K) experiment is a long-baseline neutrino oscillation experiment designed to measure several of these parameters. It consists of three main components: a dedicated beamline from the proton synchrotron main ring of the Japan Proton Accelerator Research Complex (J-PARC) that is used to produce an intense beam of muon neutrinos; a suite of near detectors situated 280 m downstream of the neutrino production target (INGRID and ND280) [1, 2] that characterize the neutrino beam before the neutrinos change flavour; and the far detector, Super-Kamiokande [3], which measures the oscillated neutrino beam. Unlike previous accelerator-based neutrino experiments [4, 5], T2K uses an off-axis configuration in which the detectors sample the neutrino beam at an angle of 2.5° to the primary proton beam, thus providing a narrower neutrino energy spectrum peaked at approximately 600 MeV which is optimized for neutrino oscillation measurements using Super-Kamiokande at a distance of 295 km downstream and assuming the current measured value of Δm^2_{32}. The ND280 is centred on the same off-axis angle as Super-Kamiokande in order to sample a similar portion of the neutrino flux that will be used to measure the oscillation parameters. The use of a near and far detector in this way reduces the systematic uncertainty on the measured oscillation parameters. The main aim of T2K is to measure θ_{13} through the appearance of ν_e in a ν_μ beam [6], and to improve the measurements of θ_{23} and the mass difference Δm^2_{32} through observation of ν_μ disappearance [7]. With recently-measured large values of θ_{13} [8, 9], T2K has a unique role to play in determining whether or not there is CP violation in the lepton sector. T2K was the first experiment to observe indications of a non-zero value for θ_{13} in 2011 [10].

The ND280 [2] is contained within the refurbished UA1 magnet, which in its current configuration provides a field of 0.2 T. The detector consists of two principal sections: the Pi-0 Detector (PØD) [11], optimized for identifying and measuring π^0 decays, and the tracker, designed for precision measurement and identification of charged particles. The tracker comprises three time projection chambers (TPCs) [12] interspersed with two fine-grained detectors (FGDs) [13] to provide target mass, surrounded by an electromagnetic calorimeter (ECal). The PØD, TPCs, FGDs and downstream ECal (Ds-ECal) are mounted in a supporting structure or 'basket' which sits inside the UA1 magnet, while the surrounding barrel- and PØD-ECal are affixed to the magnet yoke, which splits vertically as shown in figure 1 to provide access for installation and maintenance. The yoke itself is instrumented with slabs of plastic scintillator to act as a muon detector, the side muon range detector (SMRD) [14]. With the exception of the TPCs, plastic scintillator is used as the active material in all ND280 subdetectors. It should be noted that, in contrast to conventional charged-particle beams, neutrino interactions may occur at any point within the ND280 and its immediate environment.

The ND280 must provide a well-measured neutrino energy spectrum, flux, and the beam neutrino composition, as well as measurements of neutrino interaction cross-sections in order to reduce the systematic uncertainties in the neutrino oscillation parameters. This information is used to predict the characteristics of the unoscillated beam at Super-Kamiokande. Additionally, the neutrino cross-section measurements are interesting in their own right, as there are few such measurements in the literature at present.

2013 JINST 8 P10019

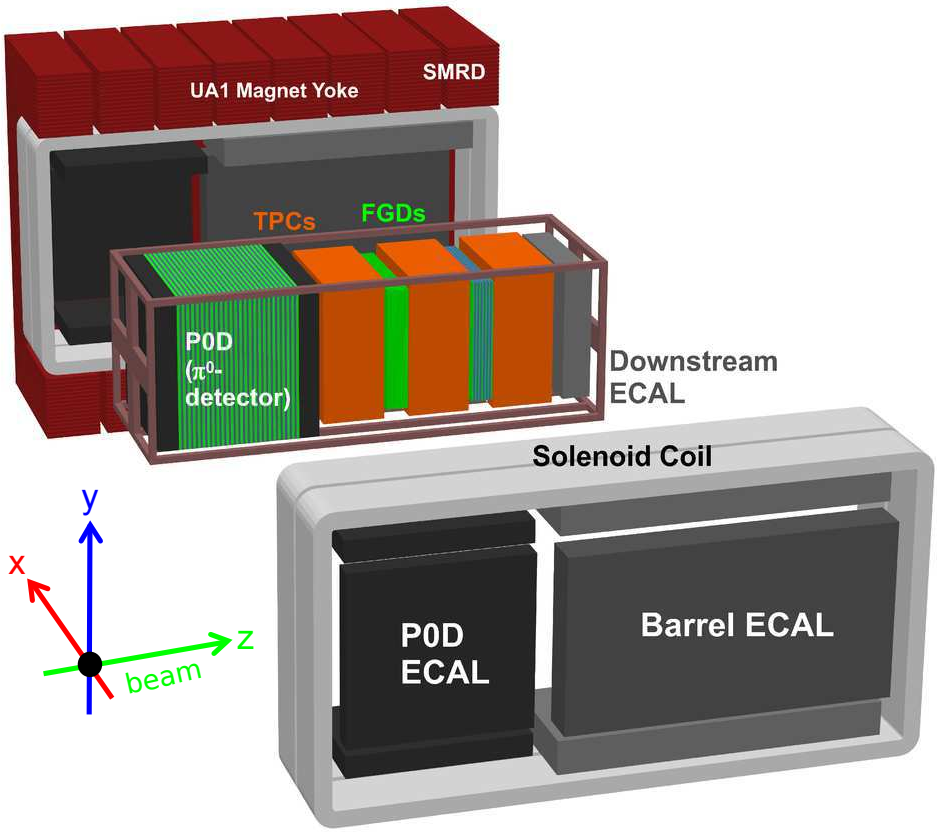

Figure 1. An exploded view of the ND280 detector, showing the PØD-ECal and barrel-ECal affixed to the magnet return yoke and the Ds-ECal mounted inside the basket. The ν_μ beam enters from the left of the figure. The detector co-ordinate system is right-handed as shown with the origin at the geographical centre, which lies near the downstream end of the first TPC.

The ECal forms an important part of the ND280 and is essential to obtain good measurements of neutral particles and electron/positron showers that lead to correct particle identification and improved energy reconstruction. It can also be used as target material to determine neutrino interaction cross-sections on lead. This paper describes the design, construction and performance of the ECal.

2 Overview of the calorimeter design

The ECal is a lead-scintillator sampling calorimeter consisting of three main regions: the PØD-ECal which surrounds the PØD; the barrel-ECal which surrounds the inner tracking detectors; and the Ds-ECal which is located downstream of the inner detectors and occupies the last 50 cm of the basket. It is often useful to consider the ECal detectors that surround the tracker region of the ND280 together; hence the barrel-ECal and Ds-ECal together are referred to as the tracker-ECal. Altogether, the ECal consists of 13 modules: 6 PØD-ECal (2 top, 2 bottom, 2 side), 6 barrel-ECal (2 top, 2 bottom, 2 side), and 1 Ds-ECal. The position of the ECal within the ND280 is shown in

2013 JINST 8 P10019

figure 1. The ECal modules that surround the barrel (barrel-ECal and PØD-ECal) are attached to the magnet and must have two top and two bottom modules in order to allow for the opening of the ND280 magnet.

Each module consists of layers of scintillating polystyrene bars with cross-section 40 mm × 10 mm bonded to lead sheets of thickness 1.75 mm (4.00 mm) in the tracker-ECal (PØD-ECal) which act as a radiator to produce electromagnetic showers and which provide a neutrino-interaction target. The size of the ECal is constrained by its position between the basket and the magnet. A larger ECal would necessitate a smaller basket and thus smaller inner subdetectors. A scintillator bar thickness of 10 mm was chosen to minimize the overall depth of the ECal while still providing sufficient light to produce a reliable signal. Scintillator bar widths, lead thickness and the number of layers per module were optimized for particle identification and tracking information. Smaller bar widths are favoured for tracking information, and optimization studies indicated that the π^0 reconstruction efficiency becomes seriously compromised for widths greater than 50 mm; hence, 40 mm was chosen as a compromise between reconstruction efficiency and channel cost. Similarly, the lead thickness of 1.75 mm was chosen based upon studies of π^0 detection efficiency. The number of layers was determined by the requirement to have sufficient radiation lengths of material to contain electromagnetic showers of photons, electrons and positrons with energies up to 3 GeV. At least 10 electron radiation lengths, X_0, are required to ensure that more than 50% of the energy resulting from photon showers initiated by a π^0 decay is contained within the ECal. This requirement is satisfied in the tracker-ECal. More information about the scintillator bars and the lead are in sections 3.1 and 3.2.

The physics aims of the tracker-ECal and PØD-ECal are somewhat different, and this is reflected in their design and construction. The tracker-ECal is designed as a tracking calorimeter to complement the charged-particle tracking and identification capabilities of the TPCs by providing detailed reconstruction of electromagnetic showers. This allows the energy of neutral particles to be measured and assists with particle identification in the ND280 tracker. To this end, there are 31 scintillator-lead layers in the barrel-ECal and 34 layers in the Ds-ECal, or approximately 10 X_0 and 11 X_0, respectively. The direction of the scintillator bars in alternate layers is rotated by 90° for 3D track and shower reconstruction purposes.

In contrast, shower reconstruction in the PØD region of the ND280 is done by the PØD itself, which consists of four, pre-assembled 'Super-PØDules', two with brass/water targets each of which provides 2.4 (1.4) radiation lengths of material when the water is in (out), and two with lead targets each of which provides 4.9 radiation lengths of material. The role of the PØD-ECal is to tag escaping energy and distinguish between photons and muons. The construction of the PØD-ECal therefore differs from that of the tracker-ECal, with coarser sampling (six scintillator layers separated by 4 mm-thick lead sheets, corresponding to approximately 4.3 X_0) and all bars running parallel to the beam direction. With only six scintillator layers, the PØD-ECal requires thicker lead sheets to ensure that photons are detected with high efficiency, that showers are well contained, and that photon showers can be distinguished from muon deposits. Simulation studies using photons and muons with energies between 65 and 1000 MeV, normally incident on a PØD-ECal face, were used to determine the optimum lead thickness. A thickness of 4 mm was found to provide good photon tagging efficiency ($> 95\%$ for photons above 150 MeV) and good μ/γ discrimination while minimizing the number of photons that are detected only in the first layer, and might therefore be rejected as noise [15].

2013 JINST 8 P10019

Table 1. Summary of the ECal design showing the overall dimensions, numbers of layers, length and orientation of scintillator bars, numbers of bars, and lead thickness for each module.

	DS-Ecal	Barrel ECal	P0D ECal
Length (mm)	2300	4140	2454
Width (mm)	2300	1676 top/bottom	1584 top/bottom
		2500 side	2898 side
Depth (mm)	500	462	155
Weight (kg)	6500	8000 top/bottom	1500 top/bottom
		10000 side	3000 side
Num. of layers	34	31	6
Bar orientation	x/y	Longitudinal and Perpendicular	Longitudinal
Num. of bars	1700	2280 Longitudinal top/bottom	912 Longitudinal top/bottom
		1710 Longitudinal sides	828 Longitudinal sides
		6144 Perp top/bottom	
		3072 Perp sides	
Bars per layer	50	38 Longitudinal top/bottom	38 Longitudinal top/bottom
		57 Longitudinal side	69 Longitudinal sides
		96 Perp top/bottom/sides	
Bar length (mm)	2000	3840 Longitudinal	2340 Longitudinal
		1520 Perp top/bottom	
		2280 Perp sides	
Pb thickness (mm)	1.75	1.75	4.0

Each scintillator bar has a 2 mm-diameter hole running longitudinally through the centre of the bar for the insertion of wavelength-shifting (WLS) fibres. Light produced by the passage of charged particles through the bars is collected on 1 mm-diameter WLS fibres and transported to solid-state photosensors, known as multi-pixel photon counters (MPPCs) [16]. The Ds-ECal WLS fibres are read out from both ends (double-ended readout); the barrel-ECal modules have a mix of double- and single-ended readout; and the PØD-ECal modules have single-ended readout. The fibres that are read out at one end only are mirrored at the other end with a vacuum deposition of aluminium. The WLS fibres and MPPCs are discussed more fully in sections 3.3 and 3.4, respectively. Each layer in each module is encased in a 20.0 mm wide $\times$ 12.5 mm high aluminium border with holes to allow the WLS fibres to exit the layer.

A summary of the ECal design is shown in table 1. Further explanation is given in the following subsections and in section 4. Figure 2 shows one complete side of the ECal in situ. The PØD-ECal is on the left and the barrel-ECal is on the right in the figure. Visible are the top, side and bottom modules for each. Notice that the PØD-ECal is thinner than the barrel-ECal as described above.

2.1 The downstream ECal

The first detector to be constructed and commissioned was the Ds-ECal, which also acted as a prototype. The outer dimensions of the Ds-ECal are 2300 mm high $\times$ 2300 mm wide $\times$ 500 mm long

2013 JINST 8 P10019

Figure 2. One entire side of the ECal in situ installed in the ND280. The three PØD-ECal modules are on the left in the figure, the three barrel-ECal modules are on the right. Part of the magnet yoke (top, red) is visible.

(depth in the beam direction). Each of the 34 layers has 50 scintillator bars of length 2000 mm. The bars of the most-upstream layer run in the x-direction (horizontally) when the module is installed in the ND280 basket. Surrounding the 34 layers on all four sides are 25 mm-thick aluminium bulkheads, which have holes for the WLS fibres to exit. Once outside the bulkhead, each end of every fibre is secured inside a custom-made Teflon ferrule as discussed in section 3.5 and shown in figure 11, which is then covered by a matching sheath that allows the WLS fibre to make contact with the protective, transparent, resin coating of the MPPC. This contact is maintained by a sponge-like spring situated behind the MPPC that can absorb the effects of thermal expansion and contraction in the WLS fibres. The sheath also contains a simple printed circuit board which couples the MPPC to a mini-coaxial cable that carries the information between the MPPC and the front-end electronic cards. Figure 3 shows the top barrel-ECal module during construction. The fibre ends in the ferrules are visible protruding from the module bulkheads. The electronics are described in section 5. The ferrule is designed to latch into the sheath which is then screwed to the bulkhead in order to hold the ferrule and WLS fibre in place, and to assure that the coupling between the WLS fibre and the MPPC is secure. The MPPC-WLS fibre coupling is described in section 3.3.

There is a 1 cm gap between the layers and the bulkheads on all sides to leave space for the light injection (LI) system. The LI system, described in section 6, uses LED pulsers to deliver short flashes of light through the gap to illuminate all of the WLS fibres, allowing integrity and calibration checks to be performed.

2013 JINST 8 P10019

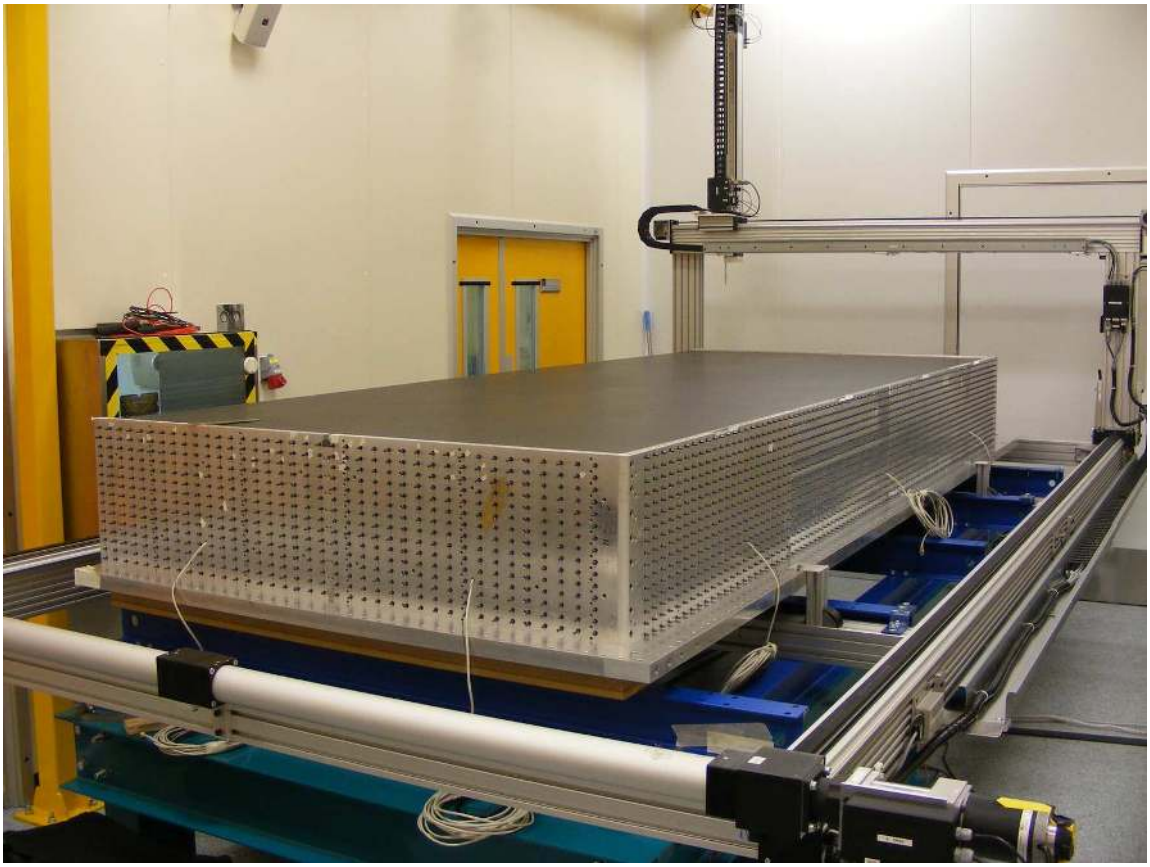

Figure 3. One of the top barrel-ECal 1.5 m × 4 m modules lying horizontally during construction. The fibre ends encased in their ferrules are visible protruding from the module bulkheads. The structure of the 2D scanner can be seen surrounding the module.

Cooling panels for temperature control are located outside the bulkheads as shown in figure 4. Pipes carrying chilled water maintain these panels at a constant temperature of approximately 21°C; the bottom panel also has perforated air pipes through which dry air is pumped to prevent condensation within the module. Large air holes through the cooling panels and the bulkheads allow the air to flush through the active region of the detector and escape from the module.

The Trip-T front-end electronic boards (TFBs) are mounted on the cooling panels using screws and thermally-conducting epoxy resin; slots in the panels allow the cables from the MPPCs to pass through and terminate on the TFBs. Each TFB has 64 channels to read out MPPCs, a built-in internal temperature sensor, and a port that connects to an external temperature sensor mounted on the bulkhead near the MPPCs in order to monitor the MPPC temperatures. There are 14 TFBs per side. Figure 4 shows the left-side cooling panel with the TFBs installed.

The cooling panels are protected by anodized aluminium cover panels, while the 2000 mm × 2000 mm outer surfaces are covered by carbon-fibre panels in order to minimize the mass of these dead regions. These cover panels form the outside of the module. Each carbon-fibre panel consists of two sheets of carbon-fibre of dimensions 2059 mm wide × 2059 mm long × 1.2 mm thick. A foam layer of 22.6 mm thickness is sandwiched between the two sheets, making the entire panel

2013 JINST 8 P10019

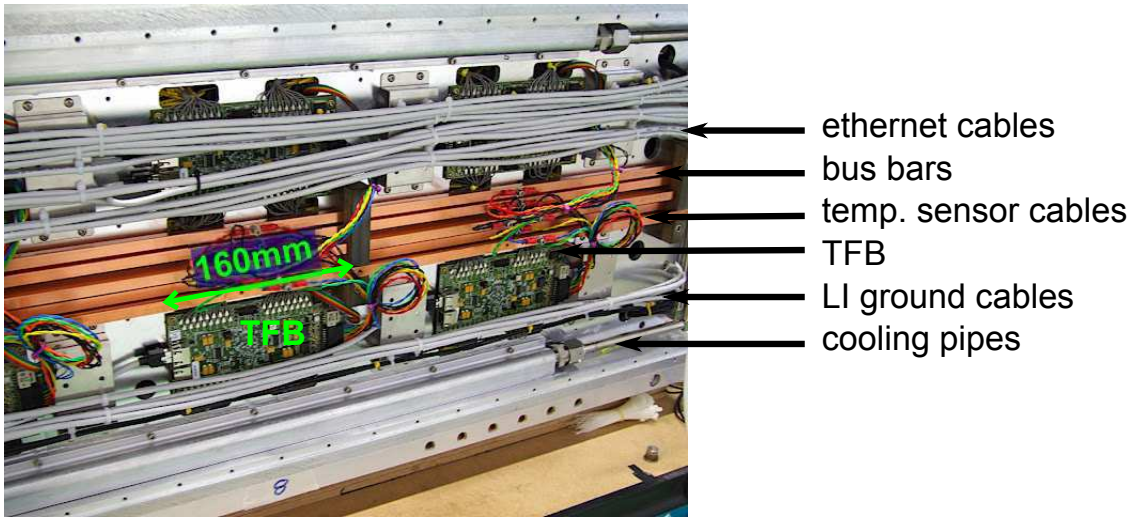

Figure 4. The left side of the Ds-ECal lying horizontally during construction. When upright in situ, the bottom in the figure becomes the upstream surface of the Ds-ECal nearest to the inner detectors, and the top in the figure becomes the downstream surface nearest to the magnet coils. Shown at the top and bottom are the Cat 5e cables (commonly used as ethernet cables), the LI cables (small, black cables at the bottom), the TFBs (green cards), the external temperature-sensor cables (multi-coloured), the cooling pipes (aluminium, top and bottom), and the bus bars (brass, centre) mounted on the cooling panels. Air holes in the cooling panel are visible on the right side of the figure. The Cat 5e cables at the top include both the signal and trigger cables; those at the bottom are signal cables.

25 mm deep. The carbon-fibre sheets are glued tongue-in-groove into an aluminium border that is 120 mm wide and 25 mm thick, making the dimensions of the entire carbon-fibre-aluminium panel 2299 mm $\times$ 2299 mm $\times$ 25 mm thick. In situ, the Ds-ECal sits upright inside the basket. Water, dry air and high-voltage enter through the bottom cover panel. The information to and from the TFBs is carried by shielded Cat 5e cables which exit through a patch panel in the bottom cover panel. In addition to these 56 signal cables, there are 28 trigger cables, routed through 28 cable glands in the top cover panel of the module, which come from the TFBs that are connected to the MPPCs located near the downstream edge of the module. Data from these channels form part of the ND280 cosmic ray trigger. Upon exiting the cover panels, the signal Cat 5e cables are connected to the readout merger modules (RMMs) which are attached to the outer surface of the cover panels. The RMMs are discussed in section 5. The trigger cables are connected to fan-in cards on the top of the module. The Ds-ECal is the only ECal module which forms part of the ND280 cosmic ray trigger system.

2.2 The barrel ECal

The four barrel-ECal top and bottom modules are 4140 mm long (parallel to the beam) $\times$ 1676 mm wide $\times$ 462 mm high, with 31 lead-scintillator layers: 16 (including the innermost layer) with 1520 mm-long scintillator bars running perpendicular to the beam direction, and 15 with 3840 mm-long bars running longitudinally, i.e. parallel to the beam direction.

The structure of each of the ECal modules is very similar to that described above for the Ds-ECal, except that the perpendicular bars have single-ended readout, with the fibres mirrored on the end that is not read out. The mirrored ends of the fibres terminate just inside the scintillator bars,

2013 JINST 8 P10019

whereas the ends that are read out exit through the bulkhead as in the Ds-ECal. The longitudinal bars all have double-ended readout.

In order to minimize the non-active gap in the ECal running down the centre of the ND280 between the two top or the two bottom modules, the mirrored ends of the fibres in the perpendicular bars are in the centre of the ND280 and the readout ends are at the sides. This made it possible to replace the thick aluminium bulkhead, cooling panels and cover panels that form the structure on the other three sides of each module with a thin aluminium cover panel, allowing the two top and the two bottom modules to be placed closer together and minimizing the dead material between them.

The two side barrel-ECal modules are 4140 mm long $\times$ 2500 mm wide $\times$ 462 mm deep, with 31 lead-scintillator layers: 16 (including the innermost layer) with 2280-mm-long scintillator bars running perpendicular to the beam direction, and 15 with 3840-mm-long bars running longitudinally, i.e. parallel to the beam direction. As in the top and bottom barrel-ECal, the perpendicular bars are single-ended readout, with the mirrored ends of the fibres at the top and the readout ends at the bottom of the modules.

Unlike the Ds-ECal which has carbon-fibre panels on both the most upstream and downstream faces, the barrel-ECal modules have a carbon-fibre panel on the innermost face, but the outermost face has an aluminium panel which provides the required structure for attaching the module to the magnet yoke.

2.3 The PØD ECal

The most noticeable difference between the tracker-ECal modules and the PØD-ECal modules is the smaller size of the PØD-ECal, which has six scintillator-lead layers and is only 155 mm deep. The four top/bottom modules are 1584 mm wide, the two side modules are 2898 mm wide, and all six are 2454 mm long. The PØD-ECal also required thicker 4 mm lead sheets as a consequence of having fewer layers. All of the scintillator bars, 38 in each top/bottom module layer and 69 in the side layers, are oriented parallel to the beam, read out on the upstream end and mirrored on the downstream end. The smaller size also allowed simplifications to be made in the construction.

While the readout electronics of the tracker-ECal detectors were mounted on separate cooling plates, the PØD-ECal TFBs are attached directly to the upstream bulkhead as shown in figure 5. This bulkhead extends 100 mm above the height of the main detector box so that the TFBs can be mounted next to the region where the optical fibres emerge. The water cooling pipes are then recessed into grooves running along the exposed face behind, through which the dry air system also passes. Because there are no more than seven TFBs in any one module, the boards could have their power provided via standard copper cables instead of the bus bars used in the tracker-ECal. The readout region was then protected by an anodized aluminium cover.

Structurally, the PØD-ECal modules used the same carbon-fibre panels as the tracker-ECal on the bases, but all had solid aluminium bulkheads to form the lids. Onto this were bolted the structures required to mount the detectors on the near detector magnet: cast aluminium rails for the side modules, and roller cages for the top/bottom modules.

2013 JINST 8 P10019

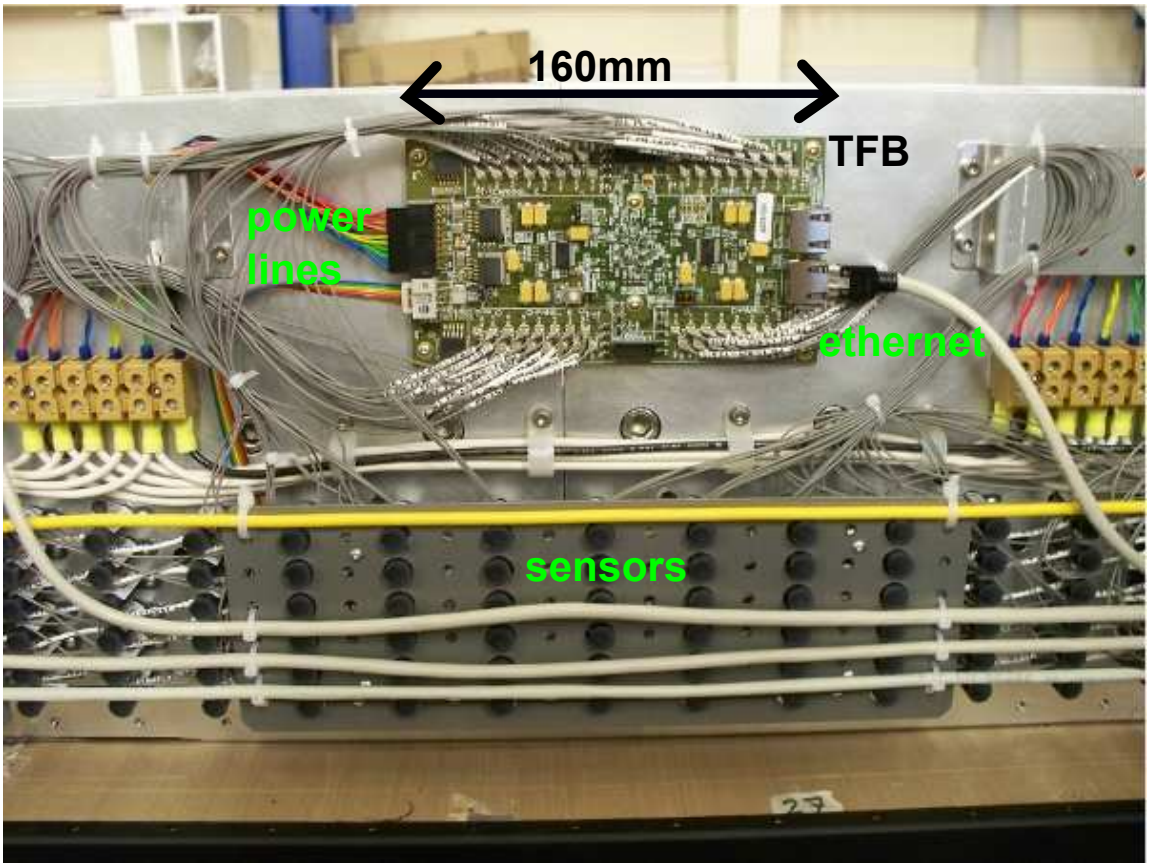

Figure 5. Closeup on the readout side of the upstream bulkhead for a P∅D-ECal side module. The black cases at the bottom house the MPPCs (photosensors) coupled to the optical fibres where they emerge from the inner detector. Each MPPC is connected via a thin grey cable to the TFB mounted above, which receives its power from the coloured cables on its left and is read via the Cat 5e (ethernet) cable on its right.

3 Materials

3.1 Scintillator bars

The ECal scintillator bars were made at the Fermi National Accelerator Laboratory (FNAL) from extruded polystyrene doped with organic fluors at concentrations of 1% PPO and 0.03% POPOP. The polystyrene scintillator bars have a 0.25 ± 0.13 mm coating of polystyrene co-extruded with TiO_2 providing light reflection and isolation. The scintillator was chosen to have the same composition as that used for the MINOS detectors [17]. Each bar has a cross-section of $(40.0^{+0.0}_{-0.4})$ mm wide $\times$ $(10.0^{+0.0}_{-0.4})$ mm deep with a 2.0 ± 0.2 mm hole running down the centre for the insertion of 1 mm-diameter WLS fibre, which is discussed in more detail in section 3.3. Each bar was cut to the appropriate length during the quality assurance (QA) process described below, to within 0.1 mm. The number of bars of each length is shown in table 1. Including the 10% extra that were made to replace any rejected during the QA process, there were a total of more than 18,300 bars shipped from FNAL.

2013 JINST 8 P10019

The scintillator bars underwent both mechanical and optical QA tests. The frequency of testing was reduced in some cases as the extrusion process at FNAL was refined due to feedback from the QA group. During the mechanical QA tests, the sizes of 100% of the bars were checked for width and thickness using custom-made Go and No-Go gauges that could slide easily along bars if the sizes were within tolerance, and a visual inspection was made for flatness and squareness. The bars were then cut to length. The hole position and diameter were checked using digital callipers for 100% of the bars for the Ds-ECal, and for 10% of the bars subsequently. Optical QA was carried out on 10% of the bars for the Ds-ECal and 5% of the bars subsequently.

For the first shipments of bars, which were used in the Ds-ECal, the hole diameter was found to vary from 1.75 mm to 3.50 mm and the shape was typically elliptical rather than round. This did not affect the light yield of the bar; however, it did have consequences for the layer construction. If the hole was too small, the locator pins used to hold the bar in place while the epoxy cured could not be inserted into the bar; if the hole was too large, glue would enter the hole around the edges of the locator pin and block the subsequent insertion of the WLS fibre. Approximately 10% of Ds-ECal bars were rejected due to this problem. Subsequent shipments of bars for use in the other ECal modules did not have this problem.

Optical QA was carried out on the scintillator bars in order to ensure a consistency of response to minimum-ionizing particles (MIPs). To this end, a cosmic ray (CR) telescope was constructed consisting of a light-tight enclosure for the scintillator bars and their photo-readout, a triple-coincidence trigger, and a simple data acquisition (DAQ) system. The bar being tested did not form part of the trigger [18].

The CR telescope consisted of three 4 cm $\times$ 6 cm scintillator pads coupled to 2-inch photomultiplier tubes (PMTs) which were biased to approximately 2 kV each. The coincidence trigger consisted of a simultaneous trigger from one scintillator pad above and two pads below the bar being tested. This criterion excluded showers and random coincidences from the PMTs and reduced the selection of CRs to those that entered the telescope at a small angle from the zenith, eliminating the need to correct for path-length differences in the bar due to differing angles of incidence. The CR telescope registered an average of 450 triggers per hour as expected from calculations.

Each bar to be tested for light yield was first wrapped in two layers of microfibre blackout material as a form of flexible dark box. In order to obtain a robust signal over the background electronic noise, the light signal of the test scintillator was collected by three 1 mm-diameter WLS fibres, rather than one, in the central hole of the scintillator bar, which was possible due to the hole diameters being larger than specified, as discussed above. The three fibres were coupled to the centre of a 2-inch PMT with optical grease to improve light transmission. The PMT was biased at a voltage of 2.55 kV.

The bar readout end was confined inside a series of plastic adaptors to enable easy replacement of the bars for testing, and to ensure a consistent, reproducible optical coupling to the PMT. A viewing port was built to enable visual verification of the coupling between the WLS fibres and the PMT, and to act as an input port for an LED-based light-injection system that was used to calibrate the single photo-electron (PE) peak in the PMT. The optical QA setup is shown in figure 6.

Output signals from the trigger PMTs were fed into a into a computer running LabVIEW that produced histograms of the charge integrals and exported the data for subsequent analysis [18]. A baseline was established using 12 scintillator bars from an early delivery. After analysis and

2013 JINST 8 P10019

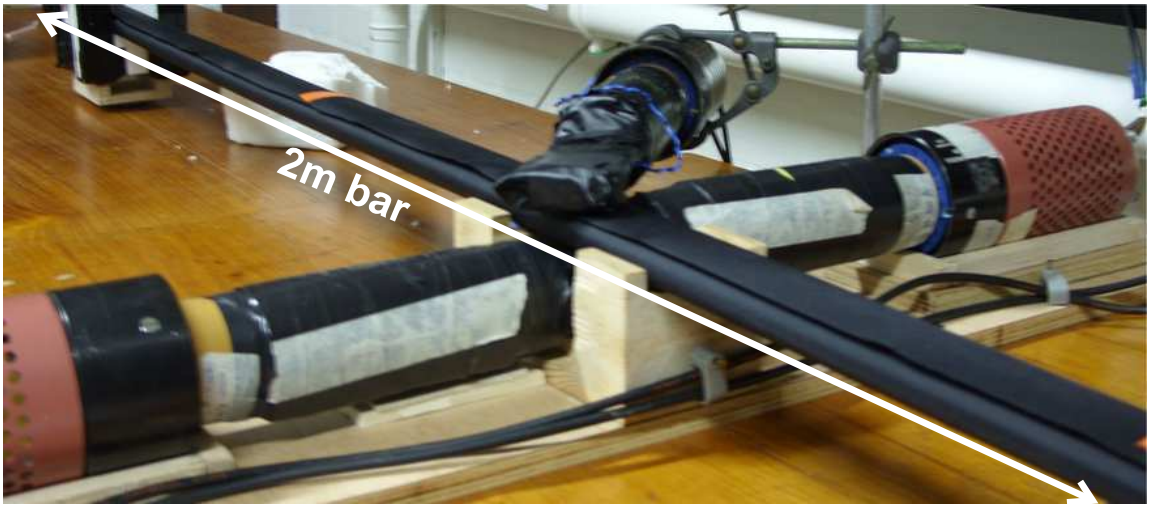

Figure 6. The CR telescope showing the 2 m-long scintillator bar in light-tight microfibre sleeve (centre) and the triple-coincidence trigger. The trigger scintillator pads are situated with one above and two below the test bar.

calibration using the single PE peak, the light yield for these 2 m bars read out at a position 66 cm from the readout end was found to be 34.2 ± 0.6 PE/MIP with $\sigma \approx 5$ PE/MIP. Bars with a light yield within 2σ of the baseline light yield were accepted. This criterion did not reject any bars.

3.2 Lead

The target mass and radiator for each layer is provided by a thin sheet of lead stiffened with $2.0 \pm 0.2\%$ antimony. Traces of other metals are below 0.15%. Each sheet of lead was coated with black, quick-drying, metal-conditioning primer, CELEROL-Reaktionsgrund 918 (Reaction Primer), before being used in a layer, in order to protect personnel from the harmful effects of lead and prevent any possibility of leaching between the lead and the scintillator which might degrade the light-yield qualities of the scintillator over time. The lead thickness for all layers in the barrel-ECal and the Ds-ECal is 1.75 ± 0.10 mm, and for the P∅D-ECal is 4.0 ± 0.3 mm. The tolerances were determined by the manufacturer and are due to the lead fabrication process. The widths and lengths differ depending upon the size of the module. Due to the technical difficulty of producing large sheets of thin lead, for the Ds-ECal and barrel-ECal each layer of lead includes more than a single sheet.

The Ds-ECal sheets upon delivery were 1008^{+4}_{-0} mm wide $\times$ 2019 ± 4 mm long and subsequently were cut to lengths of 2016 ± 1 mm during the layer construction. Two sheets were laid side by side to make up a single Ds-ECal layer.

The barrel-ECal top and bottom modules have lead dimensions 765^{+4}_{-0} mm wide $\times$ 3858^{+4}_{-0} mm long. Two sheets were laid side by side to make up a single barrel-ECal top or bottom layer. The barrel-ECal side modules have lead dimensions 2330^{+4}_{-0} mm wide $\times$ 964.5^{+4}_{-0} mm long, with the total length being provided by laying four sheets along the length of each layer.

The P∅D-ECal top and bottom modules have lead dimensions 1528^{+4}_{-0} mm wide $\times 2356^{+4}_{-0}$ mm long and the side modules have lead dimensions 2770^{+4}_{-0} mm wide $\times 2356^{+4}_{-0}$ mm long. Unlike for

2013 JINST 8 P10019

Table 2. The consignment of WLS fibres used in the ECal construction.

ECal Fibre Type	Length (mm)	Quantity	Processing
barrel-ECal Side	2343	3072	cut, ice polish, mirror one end
barrel-ECal Side/Top/Bottom	3986	4288	cut, ice polish
barrel-ECal Top/Bottom	1583	6144	cut, ice polish, mirror one end
Ds-ECal	2144	2040	cut, ice polish
PØD-ECal Side/Top/Bottom	2410	1740	cut, ice polish, mirror one end

the barrel-ECal and Ds-ECal layers, due to the thickness of these sheets it was possible to produce sheets that were wide enough for the entire layer.

3.3 Wavelength-shifting fibre

All ECal modules used Kuraray WLS fibres of the same type: Y-11(200)M, CS-35J, which are multi-clad fibres with 200 ppm WLS dye. The fibre diameter was specified to be $1.00^{+0.02}_{-0.03}$ mm. The fibres were delivered for processing as straight 'canes' to the Thin Film Coatings facility in Lab 7 at FNAL. All fibres were cut to length with a tolerance of ± 0.5 mm and both ends were polished in an ice-polishing process where a batch of around 200 fibres at a time (800 fibres per day) were diamond-polished using ice as a mechanical support. The PØD-ECal fibres and shorter fibres from the barrel-ECal modules were then 'mirrored' on one end in batches of 800 – 1000 using an aluminium sputtering vacuum process, maximizing the amount of light available to be read out from the opposite end of the fibre and saving on double-ended readout. A thin layer of epoxy was applied to each mirrored end for protection. Table 2 summarizes the full ECal WLS fibre consignment. In total, over 17,000 fibres were processed at Lab 7 and passed through the QA process described below. This represented about a 10% contingency over the total number of fibres needed to complete construction of the ECal.

A procedure of automatic scanning of fibres was put in place primarily to identify those fibres with poor light yield that do not necessarily show obvious signs of damage by a visual inspection. A secondary function of the scanning was to measure and monitor the attenuation length of the fibres which could be used as part of the ECal calibration task. Two scanning methods were developed. The first, known as the Attenuation Length Scanner (ALS), tested fibres one at a time and performed the QA for the Ds-ECal consignment of fibres. The ALS was later replaced by the Fracture Checking Scanner (FCS) which had a faster through-put of fibres as demanded by the construction schedule but with a less precise measurement of the attenuation length. In addition, each ECal module construction centre ran a scan of all fibres within a module layer as part of the construction procedure (as described in section 4.2) in order to check that the quality had not been compromised by the installation process.

The ALS, shown in figure 7, consisted of a light-tight tube containing a scintillator bar into which the test fibre is inserted. A 5 mCi ^{137}Cs source producing 662 keV photons was mounted on a rail system underneath the tube and was able to travel over the full length of the fibre under

2013 JINST 8 P10019

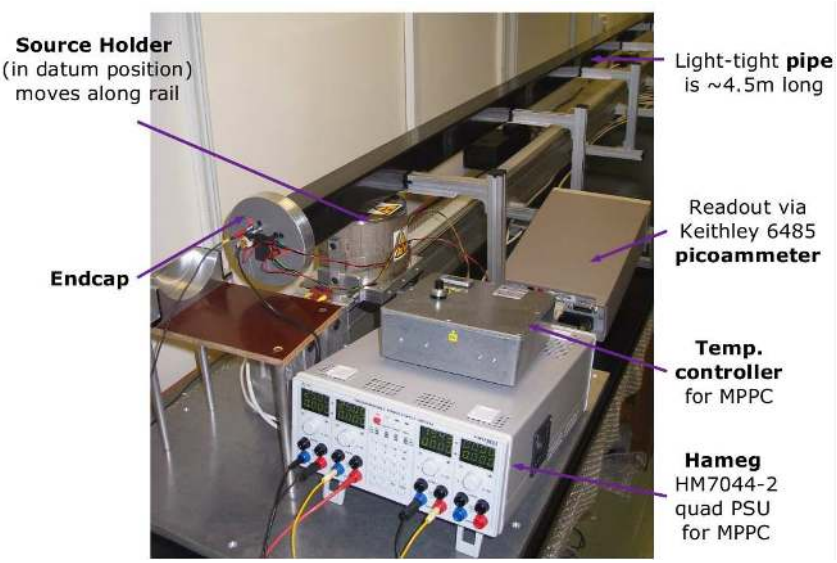

Figure 7. The ALS.

the control of a PC running LabVIEW. The light output of the fibre was recorded using a standard ECal MPPC (as described in section 3.4) powered by a Hameg HM7044-2 quadruple PSU. The output current was measured by a Keithley 6485 pico-ammeter also under LabVIEW control.

Figure 8 shows some typical results for good fibres compared to a bad fibre which shows light loss at two positions along its length (note that scans with the fibre direction reversed help to confirm the locality of the light loss). Such scans were performed on all of the fibres used for the Ds-ECal and resulted in the rejection of approximately 100 out of a total of 2000 fibres.

These data were also used in order to extract a measurement of the attenuation lengths of the fibres. An example of attenuation measurements made with this apparatus can be seen in figure 9. The current recorded from the MPPC in the region up to $x = 1.5$ m from the scan start point is fitted to the following functional form [19]:

$$I_{MPPC} = A\left(\frac{1}{(1+R)}e^{-x/\lambda_1} + \frac{R}{(1+R)}e^{-x/\lambda_2}\right) + B. \tag{3.1}$$

The data from the Ds-ECal fibres suggested a flat background of $B = 81$ nA, $A = [108, 128]$ nA, $R = [0.12, 0.14]$ and attenuation length coefficients of $\lambda_1 = [3.9, 4.1]$ m, $\lambda_2 = [0.21, 0.31]$ m.

The FCS, shown in figure 10, was designed to scan twenty fibres quickly in a single run while still retaining a reliable identification of problem fibres. The scanner was enclosed within a light-tight box with the readout electronics positioned outside. A series of 29 scintillator bars were placed perpendicular to the fibre direction and positioned over a distance of 4 m. The spacings of the bars were selected to ensure that all of the four lengths of fibre had a scintillator bar within 5 cm of the end of the fibre. Each scintillator bar was cut with 20 v-shaped grooves into which the fibres were laid allowing absorption of light from the bars.

Each scintillator bar was illuminated using an ultra-violet LED that was coupled to a 'leaky fibre', one with the cladding intentionally scratched to allow light to escape at points along the length, that was threaded through the bar. The UV light was absorbed by the scintillator bar which

2013 JINST 8 P10019

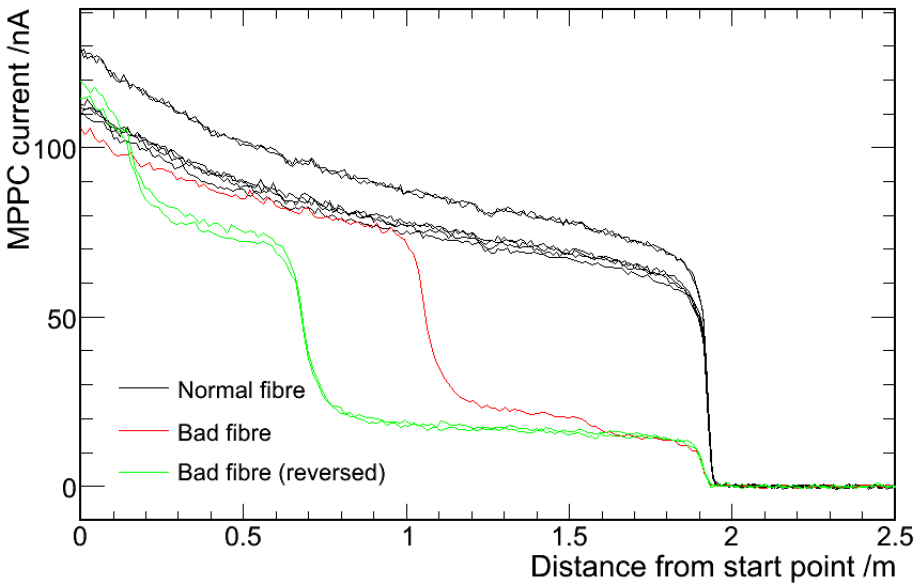

Figure 8. Some example ALS results of normal fibres compared to a fibre exhibiting light loss.

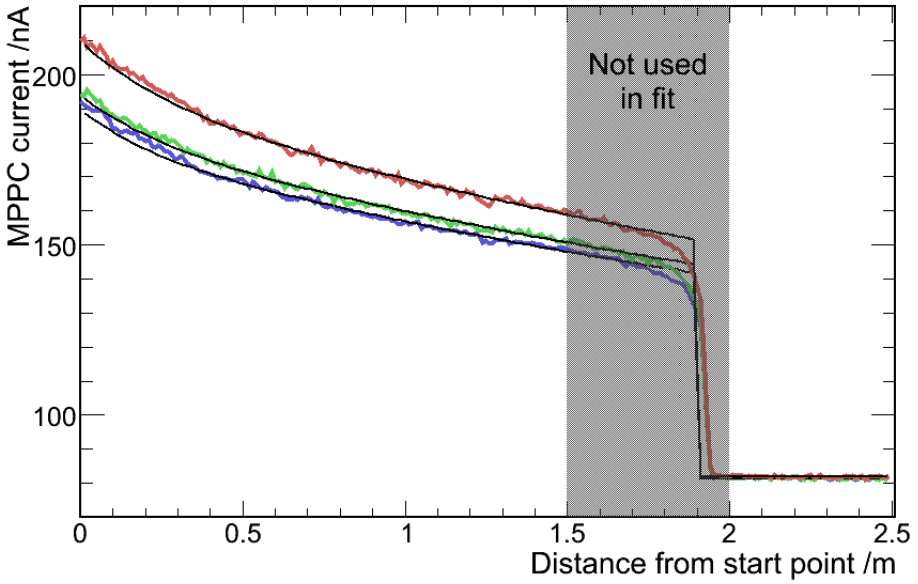

Figure 9. Example fits to attenuation length data taken by the ALS. Coloured, jagged lines are data; solid, black lines are the fits. The shaded grey region is not used in the fits.

then emitted blue light out through the v-shaped grooves and into the WLS fibres. The UV LEDs were connected to a computer-controlled switching unit that used a binary addressing system to switch on each of the LEDs in turn. The 20 WLS fibres were each coupled to ECal MPPCs which were read out via a multiplexer by the pico-ammeter. The complete scanner system was controlled by a single LabVIEW process.

2013 JINST 8 P10019

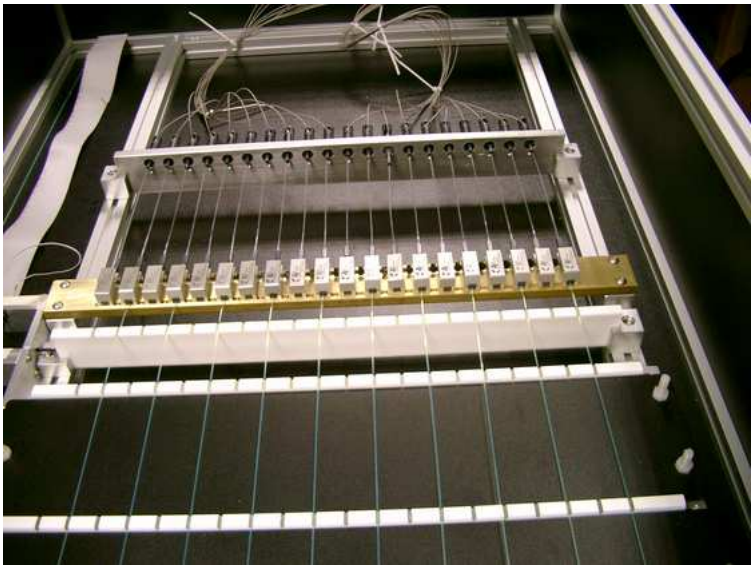

Figure 10. The FCS. Ten wavelength shifting fibres can be seen lying in the grooved scintillator bars. The fibres connect to the MPPCs (shown in their black plastic housings) via a fibre clamp and a short section of clear optical fibre. The electronics are positioned behind the far end of the light-tight box.

Software was used to check the WLS fibres for sudden drops in light output between each of the illumination points, an indication that the fibre was cracked or damaged in some way. One of the 20 WLS fibres in each run was a reference fibre that had been scanned in the ALS. A reference fibre was used for two reasons. Firstly, it allowed the scanner to be calibrated such that the expected amount of light collected at each position along the bar was known, allowing the WLS fibres to be compared to the reference fibre. Secondly, it permitted the attenuation length to be roughly measured by scaling the attenuation profile of the reference fibre with the relative light response from the other fibres. The final yield from the QA steps of WLS fibres delivered from FNAL, including any rejections due to the ferrule gluing step described in section 3.5, was 350 fibres rejected from the total order of approximately 17,000, a rejection rate of about 2%.

3.4 Photosensors

As mentioned in section 2, light produced in the scintillator bars is transported via WLS fibres to solid state photosensors. Because the ECal modules sit inside the iron return yoke of the refurbished UA1 magnet, either the photosensors needed to work inside the 0.2 T magnetic field provided by the magnet and be small enough to fit inside the ECal modules, or the light signal would need to be transported several metres via optical fibres to light sensors outside the ND280. The use of MPPCs instead of traditional PMTs allowed the first option to be chosen. MPPCs consist of many independent sensitive pixels, each of which operates as a Geiger micro-counter. The use of Geiger-mode avalanches gives them a gain similar to that of a vacuum PMT. The output of the device is simply the analogue sum of all the fired pixels, and is normally expressed in terms of a multiple of the charge seen when a single pixel fires, sometimes referred to as a 'pixel energy unit', or PEU. A customized 667-pixel MPPC, with a sensitive area of $1.3 \times 1.3\,\mathrm{mm}^2$, was developed for T2K by Hamamatsu [20].

2013 JINST 8 P10019

Table 3. Main parameters of the T2K MPPCs. The dark noise rate is given for a threshold of 0.5 PEU, or half the charge of a single pixel firing.

Parameters	
Number of pixels	667
Active area	$1.3 \times 1.3\,\mathrm{mm}^2$
Pixel size	$50 \times 50\,\mu\mathrm{m}^2$
Operational voltage	$68 - 71$ V
Gain	$\approx 10^6$
Photon detection efficiency at 525 nm	26-30%
Dark rate above 0.5 PEU, at 25°C	≤ 1.35 MHz

In addition to meeting the above criteria, the MPPCs have a higher photon detection efficiency (PDE) than PMTs for the wavelength distribution produced by the WLS fibres. Typical PDEs are given by Hamamatsu for S10362-11-050C MPPCs [21], which are similar to the customized MPPCs used by T2K. The peak efficiency, which is at a wavelength of 440 nm, is around 50%, and at the wavelengths emitted by the WLS fibres (peaked around 510 nm), the efficiency is approximately 40%. However, these PDE measurements were made using the total photocurrent from the MPPC, and will therefore count pulses caused by correlated noise such as crosstalk and afterpulsing in the same way as those due to primary photons. More sophisticated analyses performed by T2K in which these effects are removed give PDEs of 31% at wavelengths of 440 nm, and 24% in direct measurements of WLS fibre light [22]. Table 3 shows the main parameters of the MPPCs. More information about the MPPCs can be found in references [2, 13, 16, 23] and references therein.

As T2K was the first large-scale project to adopt MPPC photosensors, considerable effort was made to test the first batches of MPPCs before detector assembly. Device properties were measured in a test stand comprising 64 Y11 WLS fibres, illuminated at one end by a pulsed LED and terminated at the other by ferrules connected to the MPPCs under test, as described in section 3.5. MPPCs were read out using a single TFB board and a development version of the ND280 DAQ software. Two such test stands were created, and the MPPC testing (around 3,700 devices total) was divided equally between them.

The QA procedure consisted of taking many gated charge measurements for each photosensor at a range of bias voltages, with and without an LED pulse present during the charge integration gate. For each bias voltage, a charge spectrum was produced from the measurements, and analyzed in order to extract the sensor gain, similarly to the process described in section 8.1. The thermal noise rate, and contributions from after-pulse and crosstalk, were extracted from the relative peak heights in the charge spectrum, and a comparison of the signals with LED on and off permitted the extraction of the PDE; absolute calibration of the incoming light level was performed using a MPPC whose PDE had been previously measured using an optical power meter [22].

The gain curve was fitted to calculate a pixel capacitance and breakdown voltage for each device, and also the bias voltage required to achieve a nominal gain of 7.5×10^5. The PDE and noise characteristics at this gain were then interpolated, to quantify the performance of each device. All devices were found to be functional and to perform acceptably (with reference to table 3); however, a 10% contingency of sensors was ordered, and so devices were rejected starting with those with the

2013 JINST 8 P10019

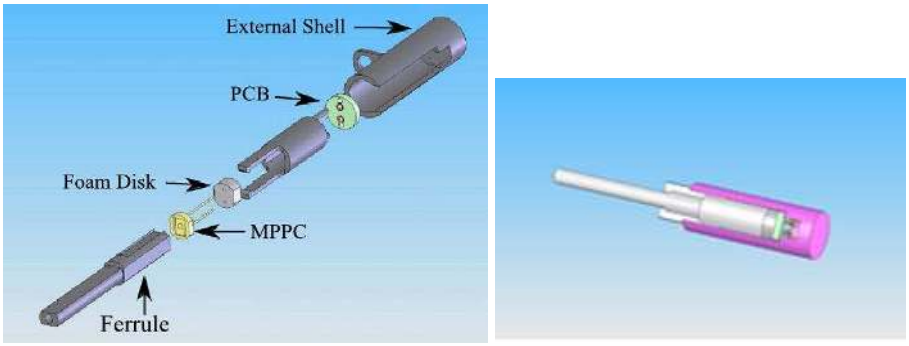

Figure 11. (Left) An exploded view of the WLS fibre to MPPC coupling connector system. The ferrule in the bottom left of the figure is placed over the end of the WLS fibre (not shown), with the fibre overhanging the ferrule by 0.5 mm in order to ensure good coupling with the MPPC. The housing for the MPPC and foam spring is shown in the centre of the figure. The 'ears' of the housing slip over the ridge in the ferrule to lock the assembly together. The external shell, or sheath, covers the MPPC housing and part of the ferrule when the connector is assembled, preventing the 'ears' from disengaging with the ferrule. The circular loop on the external shell allows the entire assembly to be screwed to the bulkhead securely. (Right) The connector fully assembled. The assembled connector is approximately 5 cm long.

highest thermal noise rate. More details on the QA procedure and its results can be found in [24]. In situ, the dominant contribution to the non-linearity of the combined scintillator/fibre/MPPC system is from the MPPCs, and is estimated to be 2-3% for MIPs and 10-15% for charge deposits typical of showers.

3.5 Fibre to sensor coupling

An essential component in the overall light-collection efficiency of the ECal modules was the coupling of the WLS fibres to the MPPCs. The design used was a multi-component solution shown in figure 11 (left) and was adopted by the on-axis INGRID detector [1] and the PØD subdetector [11] of the ND280 in addition to the ECal. The assembly consists of three injection moulded[1] parts: (1) a 'ferrule' glued to the end of the fibre which engages with (2) a housing that holds the MPPC and ensures alignment with the fibre end to better than 150 μm, and (3) an external shell, or sheath, to contain the inner assembly and provide protection. A 3 mm-thick polyethylene foam disk sitting just behind the MPPC provided sufficient contact pressure between the fibre end and the MPPC epoxy window to ensure an efficient connection without the use of optical coupling gels which could deteriorate over time and present a complicated calibration challenge. Electrical connection between the MPPC and the front-end electronics is provided by a small, circular, printed circuit board with spring-loaded pin sockets which contact the legs of the MPPC and connect to a micro-coaxial connector by Hirose (not shown in figure 11). Figure 11 (right) shows the connector fully assembled. Early prototypes of the connector revealed that an unacceptable light loss could occur if the fibre end was glued slightly short of the ferrule end. This led to the production of gluing guides which ensured a precise overhang of the fibre from the ferrule end by 0.5 mm with a high production reliability.

[1] All injection moulded components were fabricated from Vectra ®A130.

2013 JINST 8 P10019

Table 4. The ECal construction and QA model, showing contributions from Daresbury Laboratory (DL), Imperial College London, Lancaster University, Liverpool University, Queen Mary University London (QMUL), Rutherford Appleton Laboratory (RAL), University of Sheffield, and University of Warwick.

	DL	Imperial	Lancaster	Liverpool	QMUL	RAL	Sheffield	Warwick
ECal design	X			X				
Module engineering/constr.	X			X				
Ds-ECal layers			X					
Ds-ECal module			X					
barrel-ECal side layers	X							
barrel-ECal side modules	X							
barrel-ECal top/bott layers			X					
barrel-ECal top/bott modules	X			X				
P0D-ECal side layers								X
P0D-ECal side modules								X
P0D-ECal top/bott layers							X	
P0D-ECal top/bott modules								X
2D scanner					X			
MPPC QA		X			X			X
Scintillator bar QA			X				X	
WLS fibre QA								X
MPPC-WLS connectors								X
Electronics		X				X		

4 Construction

The T2K UK group employed a distributed construction model to optimize efficiency, space and the use of available personnel. Module layers were constructed first and then lowered one at a time inside prepared bulkheads, after which the MPPCs, then cooling panels, TFBs, cooling pipes, and finally cover panels were attached. The RMMs were then affixed to the outside of the modules. As each layer was installed inside the bulkheads, a two-dimensional (2D) scanner, discussed in section 4.3, carrying a 3 mCi ^{137}Cs source was used in conjunction with a well-understood set of 'test' MPPCs to check the integrity of the bar-fibre combination before the next layer was installed, enabling repairs to be made if necessary. The material preparation and QA also followed a distributed pattern. The distribution model is shown in table 4. All of the components in the table had to come together on a co-ordinated schedule for the modules to be constructed. Details of the layer and module assembly are given in the following sections.

4.1 Layer assembly

Each layer is framed by aluminium bars with an L-shaped cross-section of dimensions 20.00 mm (base) $\times$ 12.54 mm (height). The height of the base is approximately 10.2 mm, very slightly higher than the scintillator bars, and the width of the stem is 20.00 mm. Construction of the layer began by screwing the aluminium bars into place onto a Teflon-covered assembly table. The scintillator bars then were prepared by applying a two-part epoxy (Araldite 2011 Resin and Araldite 2011 Hardener) to one edge of the bars. The bars then were laid inside the layer frame such that the

2013 JINST 8 P10019

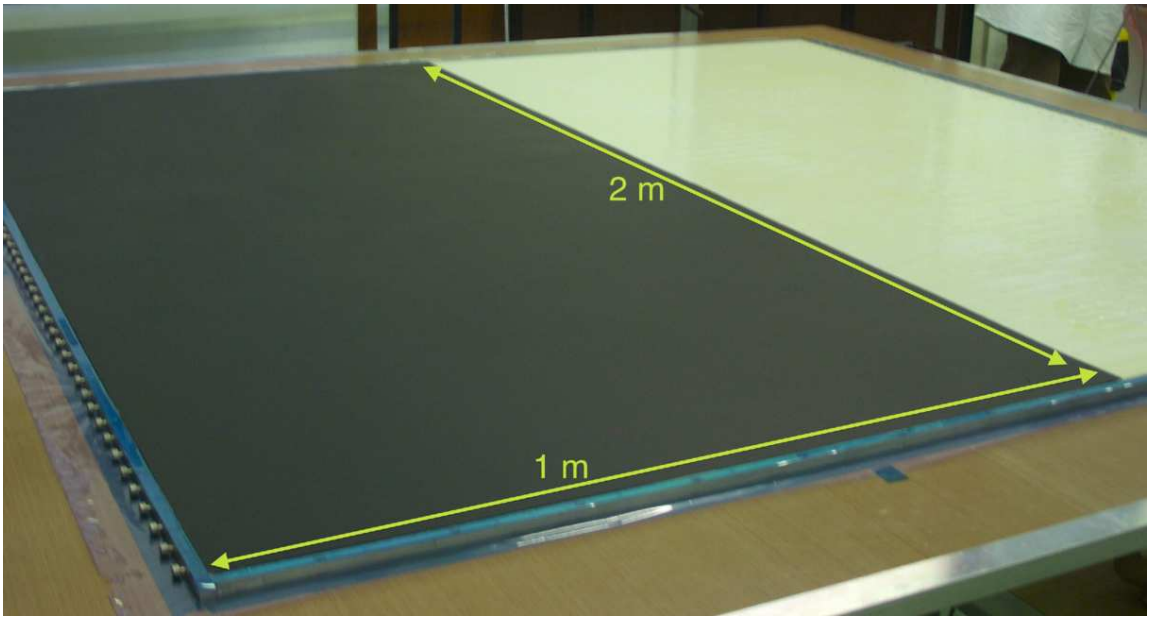

Figure 12. Ds-ECal layer under construction. The first of two sheets of lead is in place on top of the scintillator bars. Visible are the aluminium frame and the locator pins securing the scintillator bars in place for the duration of the layer construction. The frame is covered with blue tape to keep it free from epoxy.

central hole of each bar was aligned with a 2 mm-diameter hole in the frame. An O-ring with an uncompressed thickness of 1.5 mm was inserted into the 1 mm gap between the ends of the bar and the layer frame and compressed into place. This was done to prevent epoxy from entering the bar hole and compromising the subsequent insertion of WLS fibre. The position of each bar was stabilized during layer construction by inserting a temporary tapered Teflon-coated locator pin through the frame hole, the O-ring, and into the bar hole. The locator pins were removed when the layer was complete.

Once all of the bars were stabilized in position, a thin layer of epoxy was applied to them and to the lip of the frame, and the lead sheets were placed on top, using a vacuum lifting rig attached to an overhead crane in order to distribute the weight across several equally-spaced suction cups and so avoid distorting the lead. The sheets were carefully positioned to minimize the gap between them, thereby avoiding a region of low density in the middle of the modules, while ensuring sufficient overlap onto the lip of the layer frame to maintain structural integrity. Figure 12 shows one of the Ds-ECal layers being constructed, with one sheet of lead in place on top of the scintillator bars.

The entire layer then was covered with a sandwich of vacuum-sealing plastic and fabric, with the top layer of plastic securely taped to the table. Vacuum pumps were used to evacuate the air around the layer, allowing the epoxy to cure for 12 hours under vacuum compression.

Once the curing was finished, the layer was unwrapped, the locator pins removed, the screws securing the layer frame to the table were removed, the WLS-fibre holes were tested to ensure that they had not been blocked with epoxy, and the layer then was stored for use in a module.

2013 JINST 8 P10019

4.2 Assembly procedures for the ECal modules

The Ds-ECal was the first module to be constructed and most of the procedures developed during the process were used on the other modules as well. The first step was to assemble the bulkheads and the carbon-fibre panels. One carbon-fibre panel (the bottom panel during construction which would become the upstream face when the Ds-ECal was in situ) was attached to the bulkheads to form an open box. The other (top) carbon-fibre panel was stored until later. The bulkhead box was positioned on the construction table, and the 2D scanner, discussed in section 4.3, was attached and commissioned. The first layer then was lowered inside the bulkheads and positioned on top of the carbon-fibre base. A 1 cm gap between the bulkheads and the layer on all four sides was obtained by tightening or loosening grub screws which were inserted through holes in the bulkhead and tensioned against the layer frame. The LI LED strips and perspex lenses (see section 6) then were glued onto the bottom carbon-fibre panel in the 1 cm gap; the LI electronic cards were affixed to the inside of the bulkheads, with the LI cables routed outside the bulkheads through the air holes. WLS fibres were inserted through the scintillator bars. A MPPC-fibre connection ferrule was bonded to each fibre using Saint-Gobain BC600 silicon-based optical epoxy resin. The test MPPCs were coupled to the fibres using the connection sheaths and connected via a mini-coaxial cable to TFBs, which provided the control and readout (see section 5 for a description of the TFBs). After this the layer was covered and made light-tight, and a 2D scan was taken.

The 2D scanner collected data at 20 points along each 2000 mm bar, with data points being closer together near the ends in order to facilitate an understanding of the light escaping through the ends of the scintillator bar. For efficiency, the analyzing software ran in parallel with the data-taking, producing an attenuation profile for each bar in the layer. A typical example of this is shown in figure 13. The ordinate axis shows a reference value of the light yield since it is calculated as a ratio of the integrals (from 5.5 PE to 30 PE) of the MPPC response when the source is present, to the response when the source is not present, and therefore represents (signal + background)/background. This ratio is calculated at each data point along the length of the bar. More information about the analysis of the scanner data is available in [18].

The scan data were checked and if problems were encountered, appropriate action was taken. A common problem involved the coupling between the fibre and the MPPC, often due to the difficulty of positioning the ferrule on the fibre. In this case, since the ferrule could not be removed, the fibre would be replaced, a new ferrule would be attached, and the bar would be re-scanned. After this process, the test MPPCs were removed and the next layer was installed and scanned in the same manner. Where required, thin Rohacell foam sheets were placed between the layers to ensure that the layers did not warp inwards.

After several layers were installed in the Ds-ECal, it was noted that the holes in the bulkheads were no longer aligning well with the holes in the layers and the scintillator bars, which made the insertion of the WLS fibre difficult. Measurements indicated that the layer frames had been incorrectly manufactured and were an average of 0.2 mm higher than the specifications. This was remedied by using a router to thin the frames on the layers that were not yet installed. The layer frames for subsequent modules did not have this problem.

After all of the layers were installed, LI LEDs and electronic cards were attached to the top carbon-fibre panel. 9 mm of Rohacell foam was glued to the inside of the panel to ensure that the

2013 JINST 8 P10019

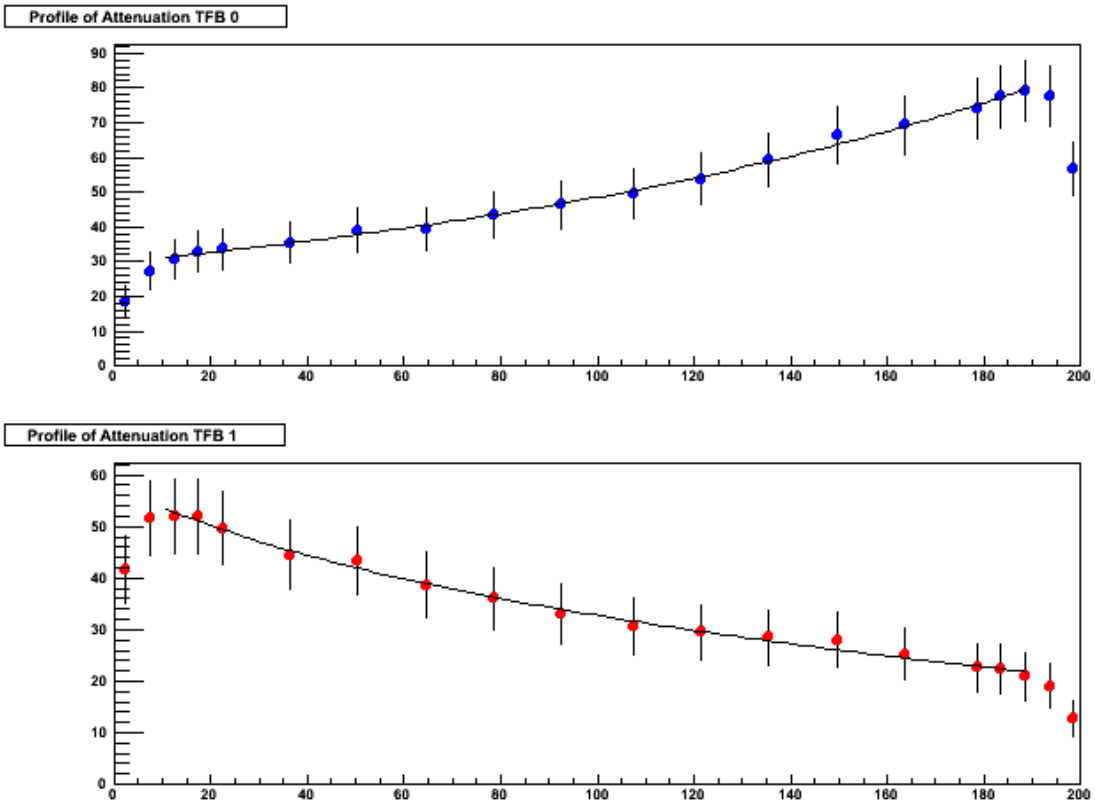

Figure 13. A typical light attenuation profile from scanner data corresponding to one scintillator bar in the Ds-ECal. The ordinate axis is the ratio of the integrated light yield with the source present to the integrated light yield without the source; the abscissa is the position along the bar in cm. The light yield measured by the MPPC at one end of the bar and read out by one of the two TFBs (TFB 0) is shown in the upper plot, and that from the MPPC at the other end read out by the other TFB (TFB 1) is shown in the lower plot. The points are data; the curves are a single-exponential fit to the central region of the data.

layers within the bulkheads stayed stable when the Ds-ECal was in its upright position in situ. The carbon-fibre panel was then affixed to the top of the bulkheads.

The procedure described above completed the construction of the active region of the detector. The next steps dealt with the data readout. First, the 3400 Ds-ECal 'production' MPPCs in their custom-made sheaths complete with foam springs and mini-coaxial cables were attached to the ferrules of every layer and secured to the bulkheads as described in sections 2.1 and 3.5. Cable-management brackets were attached to the bulkheads and the MPPC cables were grouped together and tidied in preparation for the next steps. Tyco Electronics LM92 temperature boards were screwed onto the bulkheads between the MPPCs in positions that allowed one temperature board to be connected to each TFB.

The cooling panel for the left-side Ds-ECal was assembled from four separate cooling plates. The TFBs then were attached and thermally connected to the left-side cooling panel using screws and thermally-conducting epoxy resin. The cooling panel then was held in position on the left side of the Ds-ECal while the MPPC and temperature-board cables were threaded through the slots in

2013 JINST 8 P10019

the panel and the LI cables were routed through the panel's air holes, after which the panel was placed into its final position and bolted into place. The MPPC and temperature-board cables were connected to the correct ports on the TFBs. The same procedure was followed for the other three cooling panels.

The water-cooling circuit then was installed on the cooling panels and the gas distribution branch was installed on the bottom cooling panel. These systems were tested under pressure. Following this, cable-management brackets were fitted between all of the TFBs, and low-voltage feedthroughs and bus bars were installed. The bus bars were checked for continuity, isolation from ground and from each other. Shielded Cat 5e cables then were connected to the TFBs. Along with the LI cables, they were routed around the detector to a patch panel mounted on the bottom cooling panel or, in the case of the trigger cables from the TFBs and half of the LI cables, to the top cooling panel. Figure 4 shows the left-side Ds-ECal cooling panel with the TFBs, bus bars, Cat 5e cables, LI cables, water-cooling pipes and air holes.

The outer cover panels then were attached to each side. The top cover panel was fitted with 28 cable glands through which the Cat 5e cables corresponding to the trigger system exited the detector, and with air vents to allow the gas being flushed through the detector to escape. Half of the cables from the LI system exited through holes in the top cover panel. The bottom cover panel was fitted with power cable clamps, cable-management brackets and RMM cards. The Cat 5e cables were routed from the patch panel to the RMMs. LI junction boxes were attached and connected to the LI cables, completing the construction of the Ds-ECal.

This construction procedure was repeated for each of the barrel-ECal modules. Minor alterations to the method were needed to accommodate the slightly different structure of the modules (see section 2.2). More significant alterations were made to the method for the PØD-ECal modules, reflecting their slightly different design, as described in section 2.3. The most significant differences were that the TFBs were mounted directly on the bulkhead instead of onto cooling panels, with the MPPC cables routed to them and supported where necessary; the smaller number of TFBs per module allowed for the use of a thick standard copper wire, instead of bus bars, to supply power, which was distributed to the TFBs via branching connections to terminal blocks; in the final step of the assembly, a non-magnetic support structure was bolted to the aluminium back panel, which positions the thinner PØD-ECal modules away from the magnet, and closer to the basket.

4.3 The bar scanner

Three-axis scanners were designed to position a ^{137}Cs radioactive source at multiple points above the surface of each detector layer as each layer was assembled into the subdetector body. Three variants of the scanner were manufactured:

- Ds-ECal and PØD-ECal scanner, with a footprint of 3928 mm $\times$ 3578 mm;
- side barrel-ECal scanner, with a footprint of 4862 mm $\times$ 3240 mm;
- top-bottom barrel-ECal scanner, with a footprint of 4862 mm $\times$ 2410 mm.

The three axes were driven by Mclennan SM9828 Stepper Motors controlled by PM600 Intelligent Stepper Motor Controller. The controller was programmed via a commodity PC running

2013 JINST 8 P10019

LabVIEW. The PC and stepper motors, along with their controller, were all powered via an uninterruptible power supply (UPS). The system design included an APC Smart-UPS 2200, 230 V, primarily as a safety feature so the radioactive source could be automatically parked during a power cut; however, it had the added benefit that short duration power glitches did not stop a running scan.

These controls were integrated into a LabVIEW program providing an operator interface to control the machine. This operator interface was implemented as a 'state' machine, the main states being 'source loaded' and 'source unloaded'. In the source-unloaded state the radioactive source was not attached to the scanner head. In this state the head was raised and moved to one side to position the arm in the least inconvenient position for those working on the detector. The arm could also be moved in the x-direction to allow for greater access to the detector during construction.

The source was loaded under computer control with the computer prompting the operator to perform the necessary steps in a safe order. The program then switched to the source-loaded state where scanning parameters could be input and the scan started. Each scan started with the z-arm searching for the surface of the module layer at the centre of the module. The arm descended slowly until the push rod mounted adjacent to the source operated. The arm then backed off and the source moved to the matrix of measurement positions. At each position the Scan Control program prompted the DAQ to start data-taking via a network link. On completion of data-taking, the scanner would move to the next position and iterate until data had been taken at all positions. When the data-taking was complete, or if the program detected an error condition, the source would be returned to its lead-shielded safe parked position. Unloading the source was again under computer control with operator prompts to ensure safety. Re-positioning of the scanner head was found to be accurate to within 0.02 mm.

Figure 14 shows the scanner in operation during the Ds-ECal construction. The vertical arm finds its position as described in the text. The operator provides the $x-y$ coordinates and the required timing at each position. Since radiation safety rules dictated that no one should be in the area during the scan, the image was taken by a web camera which allowed operators to check on the scanner progress.

5 Readout electronics and data acquisition

As described in section 2.1, the mini-coaxial cable from each MPPC is routed outside the cooling panels and connected to a custom designed TFB. Each TFB contains 4 Trip-T application-specific integrated circuits (ASICs), originally designed for the D0 experiment at FNAL. Up to 16 MPPCs can be connected to each ASIC, implying that a maximum of 64 MPPCs can be connected to a single TFB. In total, the ECal has 22336 electronic channels connected to MPPCs. To increase the dynamic range of the electronics, the incoming MPPC signal is capacitively split (1:10) into high- and low- gain channels, which are read by different channels of the ASIC. Depending on the MPPC gain, the single-pixel (1 PEU) signal corresponds to approximately 10 ADC counts in the high-gain channel, while the maximum signal in the low-gain channel corresponds to around 500 PEU.

The Trip-T chip integrates the charge in a preset (programmable) time interval which is followed by a programmable reset time at least 50 ns long. For T2K, the integration windows are programmed to synchronize with the neutrino beam timing. The Trip-T chip integrates from 23 readout cycles in a capacitor array and once all cycles have been completed the stored data are mul-

2013 JINST 8 P10019

Figure 14. The 2D scanner moving along the scintillator bars in the Ds-ECal. The ^{137}Cs source sits at the bottom of the vertical arm of the scanner, just above the layer being scanned. The blackout material covering the layer is seen, along with the tape holding it in place for the duration of the scan.

tiplexed onto two dual-channel 10-bit ADCs which digitize the data. Signals from the high-gain channel are routed via a discriminator which forms part of the Trip-T chip. A field-programmable gate array (FPGA) produces timestamp information from the discriminator outputs and sends this information together with the ADC data to a back-end board. In addition, the TFB also records monitoring data (e.g. temperature, voltage) via the same FPGA, which is asynchronously transmitted to the back-end board for data concentration and buffering. Detailed information about the Trip-T chip and front-end electronics is given in references [2] and [25].

The back-end electronics system for the ND280 consists of several different boards. The TFBs are connected to RMMs which provide control and readout. Control is fanned out from a master clock module (MCM), via several slave clock modules (SCMs), one per subdetector. Additionally, two cosmic trigger modules (CTMs) are used to provide a selection of cosmic-ray muon triggered events for calibration and monitoring. All of these boards use a common hardware platform, specifically developed by the Rutherford Appleton Laboratory for use in the T2K experiment. Signals from up to 48 TFBs, which are mounted on the detector typically less than 1 m away from the MPPCs, are routed to one RMM via Cat 5e cables. The ECal uses a total of 12 RMMs: 8 for the barrel-ECal, 2 for the Ds-ECal and 2 for the PØD-ECal. Each RMM controls its associated TFBs, distributes the clock and trigger signals to them and receives data from them once a trigger has been issued. Data from the RMMs are then sent asynchronously via a gigabit ethernet link to commercial PCs that collect and process the data.

The ND280 uses a single MCM. This receives signals from the accelerator which allow it to determine when a neutrino spill is about to occur, and also from a GPS-based clock which is used to synchronize the electronics to UTC. The MCM prioritizes and issues triggers across the whole

2013 JINST 8 P10019

detector, and manages readout-busy situations. The signals and control of the MCM are fanned out to the SCMs. The trigger and clock signals are passed to the ECal RMMs via the ECal SCM. The SCMs allow the electronics for a sub-system to be configured independently. It is possible for the ECal to run autonomously ('partitioned DAQ') from the rest of the ND280 for calibration and debugging by using the ECal SCM as master controller.

The software control of the detector is performed using the "Maximum Integration Data Acquisition System" (MIDAS) [26]. The front-end software is custom written to manage the communication with the RMMs, CTMs, SCMs, and MCM through gigabit ethernet links. A second process combines ADC and TDC information, compresses the data and makes histograms for pedestal determination and monitoring. A third process manages communications with computers running the MIDAS DAQ elements. These three processes co-operate on front end PCs running Scientific Linux, with each front end PC being connected to two back-end boards. The event builder and data logging use software from the MIDAS distribution with virtually no customization for T2K. The DAQ contains an online monitoring system which makes histograms for assessing data quality in real time and passes events to the online event display for monitoring. Detailed information about the DAQ is given in [2].

6 Light injection system

The ND280 ECal LI system is designed to provide a quick and reliable method of monitoring the performance of the MPPCs used inside the ECal modules. A complete discussion of the LI system R&D can be found in reference [27]. The LI system is required to illuminate the MPPCs on a given readout face of an ECal module, with a short duration optical pulse. The pulse length and stability must be sufficient to afford accurate (≈ 1 ns) timing calibration. The intensity across the readout-face should be uniform and any electromagnetic or electro-optical noise induced by the system must not interfere with the surrounding sensors or electronics.

In order to accomplish these aims, the LI system employs a modular design incorporating dedicated electronics for both the interface with the ND280 DAQ and the pulsing of LI sources within an ECal module. The components are described in the subsections that follow. The LI front-end electronics are housed in custom-built crate assemblies compatible with a standard 19-inch rack. In brief the LI signal chain comprises the following components:

1. The trigger card receives the ND280 MCM signal.

2. Control cards (CCs) receive and interpret the DAQ instructions and collate with the clock.

3. The junction boxes (JBs) receive and fan out the CC outputs.

4. The pulser receives the CC output via a JB and drives LED strips which emit optical pulses for calibration.

Each of the components is described in more detail below.

2013 JINST 8 P10019

6.1 Control cards and trigger receiver

The LI system receives DAQ instructions into a dedicated CC. Each card hosts a TCP/IP server that allows the DAQ instructions to be interpreted and then encoded into a sequence of TTL pulses used to drive LED pulser cards, housed inside the ECal modules. The ND280 MCM transmits a 100 MHz signal to the LI system which is received by a dedicated trigger card. The clock signal is first fanned out to each CC, then collated with the CC outputs onto a RJ45/Cat 5e signal cable ready for distribution to the LI JBs.

6.2 Junction boxes

The JBs are responsible for directing the TTL pulse train and MCM clock from the CCs to the relevant LI pulsers, the pulser being the dedicated electronics required to form the electrical excitation pulses used to drive the LED strips used for illumination. There is one JB per ECal module except for the Ds-ECal which has two: $6\times$ P∅D-ECal, $6\times$ barrel-ECal and $2\times$ Ds-ECal, making 14 in total. The JBs are mounted outside, but in close proximity to, the ECal modules themselves. They are passive devices, used exclusively for fanning out the CC pulses and therefore introducing no modification to the actual signal.

6.3 Communications protocol and cabling

The low-voltage differential signalling (LVDS) protocol is used throughout to ensure robustness against interference from electromagnetic noise in the detector. The DAQ instruction and MCM clock information are received over LVDS, converted to TTL for interpretation by the CCs. The CC outputs are again transmitted using LVDS, converted to TTL for fan out in the JBs and then transmitted to the LI pulsers again using LVDS. The Ds-ECal portion of the LI system, however, is an exception in that it features an older design which implements TTL over LEMO cables rather than LVDS over RJ45/Cat 5e cables. In order to preserve the relative timing between pulsers, all Cat 5e/LEMO cables within an ECal module have been installed with the same length.

6.4 Pulsers

LED pulser cards mounted inside the ECal modules receive the pulses emitted from the CCs via the JBs. The TTL logic pulses determine the pulse duration, amplitude and number of flashes. A shaping component of the pulser board introduces activation and deactivation spikes to the leading and trailing edges of a square-wave electrical pulse. This ensures a constant level of illumination with a negligible optical rise time. The signal chain is illustrated in figure 15. Different numbers of pulsers are located in different ECal modules, depending on their size and layout. There are 114 in total: 14 P∅D-ECal, 84 barrel-ECal and 16 Ds-ECal.

6.5 LED strips and extruded perspex lens

Each LED pulser drives two KingBright LSL-062-05 flexible LED lighting modules. The LED strips are fitted with an optically coupled, cylindrical lens, made of 2 mm-diameter extruded perspex, as shown in figure 16. The KingBright LEDs feature an in-built lens with $1/2$ angle 120° producing a rather wide beam divergence that results in a 75% loss of emission at the layers furthest from the LED strips. The addition of the perspex rods focuses the light so as to reduce this loss to only 25% of the maximum.

2013 JINST 8 P10019

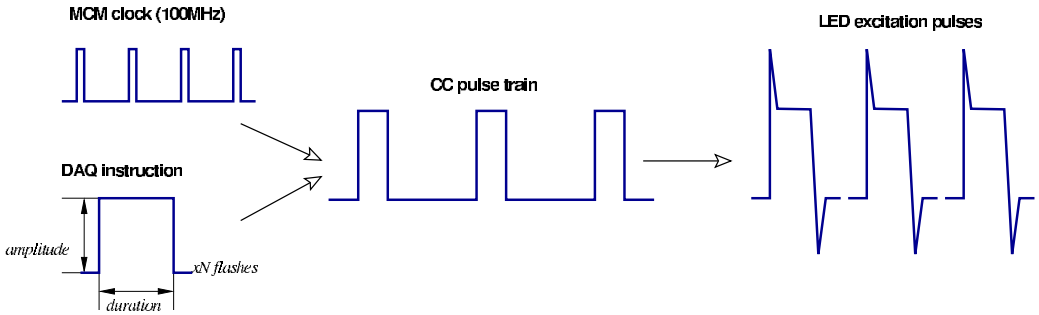

Figure 15. The LI signal path. The CCs encode an MCM synchronized pulse train with the desired timing and amplitude characteristics. The pulsers derive the excitation charges from the CC output.

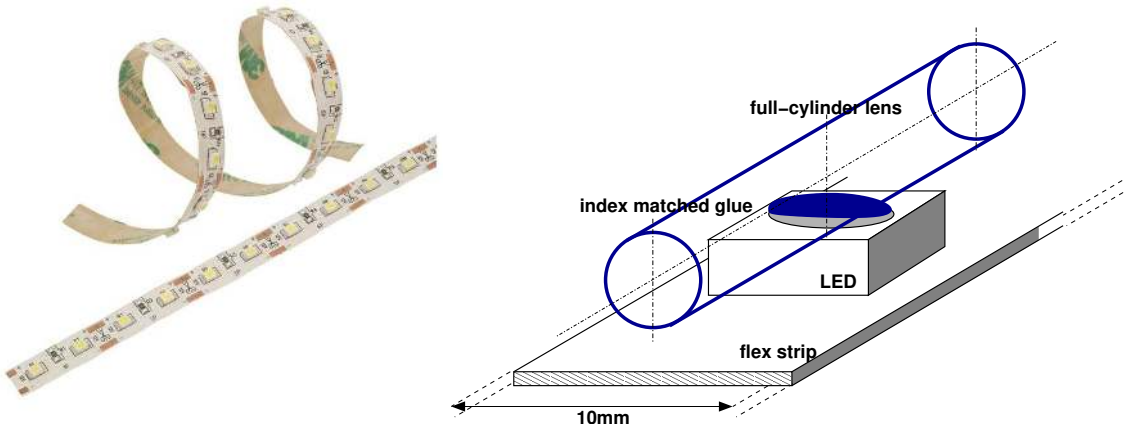

Figure 16. KingBright LED 10 mm-wide strip (left), and optically-coupled acrylic lens (right).

6.6 LI installation

The Ds-ECal JBs were installed and cabled in Aug 2010. The remainder of the JBs and the front end electronics were installed during Oct/Nov 2010.

The PØD-ECal CC receives : $1\times$ input from the DAQ.
The PØD-ECal CC transmits : $1\times$ output to each of six JBs.

A single PØD-ECal CC, located in the LI electronics crate, transmits the DAQ instructions and MCM clock information to the six PØD-ECal JBs. Each JB splits and distributes the instructions and clock information to $14 = 4 \times 2$ pulsers $+ 2 \times 3$ pulsers forming six groups, permitting any combination of the six PØD-ECal modules to be illuminated.

Each barrel-ECal CC receives : $1\times$ input from the DAQ.
Each barrel-ECal CC transmits : $2\times$ outputs to each of six JBs.

There are six barrel-ECal CCs in total. One barrel-ECal CC transmits the DAQ instructions and MCM clock information to one barrel-ECal JB over two RJ45/Cat 5e cables. One JB splits and distributes the instructions and clock information to 14 pulsers, forming three distinct groupings, each corresponding to pulsers located on one of the three readout faces. Any combination of

2013 JINST 8 P10019

readout faces (i.e. the ends of the single and double-ended scintillator bars) can be illuminated within a given barrel-ECal module.

The Ds-ECal JBs are unique in that they sit inside the ND280 magnet, situated directly against the ECal bulkheads. Moreover they employ LEMO connections along single core coaxial cable rather than the RJ45/Cat 5e that is ubiquitous elsewhere throughout the ECals and the remainder of ND280. There are two readout faces per Ds-ECal module each separately illuminated by eight pulsers. There are two JBs, one North and one South served by a single CC situated in the LI front-end electronics crate.

7 Testbeam

In 2009, the Ds-ECal module was exposed to the CERN T9 testbeam. This represented the first opportunity to test the entire integrated system: calorimeter, readout system, DAQ system and analysis framework. As well as a system shakedown, the data provided by the testbeam have been used to tune the particle identification algorithms used in T2K analyses and to obtain a better understanding of detector performance.

7.1 The CERN PS T9 testbeam

The T9 beamline is a medium energy, multiple particle species, tertiary beam generated by the collision of protons from the CERN PS on a solid target in the CERN East Experimental Hall. The dual polarity beam supplied a mix of pions, electrons and protons with momenta ranging from 300 MeV/c up to 15 GeV/c. Data were taken at momentum points between 300 MeV/c and 5.0 GeV/c. The particle composition of the beam changed with momentum setting. Below 1 GeV/c, electrons made up 90% of the beam. This fraction decreased to approximately 5% for momentum settings above 3.0 GeV/c, with a corresponding increase in the fraction of hadrons.

7.2 Triggering and event selection

The beamline was instrumented with several detectors to provide particle identification information. Two Čerenkov counters filled with CO_2 at variable pressure were present, and read out using PMTs connected to an ordinary TFB board. The counters were configured such that only electrons were above threshold, which provided electron/hadron discrimination. The electron identification efficiency of the system (requiring both counters to register a hit) was estimated to be $(90 \pm 2)\%$ for momentum settings below 3.0 GeV/c. The Čerenkov system was complemented by a time-of-flight (TOF) system comprised of two scintillator paddles read out by fast PMTs. The paddles were separated by a flight distance of 14 metres. Custom NIM-based electronics, including a time-to-analogue converter (TAC), converted the time of flight to a current pulse, which was read out using a TFB. The TOF system provided proton-pion separation for momentum settings between 600 MeV/c and 1.8 GeV/c, and also acted as the hardware trigger for the Ds-ECal.

Combining the performance of the TOF and Čerenkov systems with the beam composition, the contamination of the hadron sample with electrons was estimated to be below 0.5%, and the electron sample was estimated to be more than 99% pure. Because of the relative timings of the physics signal and DAQ cycle, the physics data from a single beam event could fall into one of two Trip-T integration windows. Due to latencies in the system it was also possible that different parts

2013 JINST 8 P10019

of a single event could end up spread across different time buckets. In this case it was impossible to be sure that activity did not occur, undetected, during the reset period. To eliminate this uncertainty, events with reconstructed clusters in both windows were rejected. For electron events, the candidate cluster was also required to arrive between 0 and 65 ns after the Čerenkov signal.

7.3 Detector configuration

The detector was configured as similarly as possible to its final operating conditions; however, there were some differences, largely due to physical constraints. The downstream end of the detector (with respect to the J-PARC beam) faced upstream in the testbeam, meaning that incident particles passed from the back to the front of the detector. This meant that the particles passed through a lead layer before a scintillator layer, leading to a small difference in behaviour.

In addition to this, the detector was cooled using an air-based chiller rather than water cooled, leading to a diurnal variation in temperature of around 2°C, and a total temperature range of 16–28°C over the whole running period. This led to rather larger drifts in MPPC behaviour than expected for the final system, leading to some difficulties in calibration (section 7.4), though after an initial commissioning period these were mostly ameliorated by taking very regular calibration runs.

7.4 Calibration differences

Calibration for the testbeam was carried out using only dedicated pedestal runs rather than using noise spectra as in the final calibration scheme, described in section 8.1. Initially, pedestal runs were taken infrequently, but after examining the early data we noticed that this was not sufficient to fully calibrate for the effect of the large temperature variations in the T9 setup. We therefore changed operating procedure to take a dedicated pedestal run before every physics run. For operations at J-PARC, we have added the ability to take interspersed pedestal data and measure noise spectra during normal running, reducing the need for these dedicated runs. The more sophisticated cooling system at J-PARC also reduces the need for very frequent calibration.

To improve the calibration of early data, we made use of the fact that the average temperature of the detector was measured at the start of each run. The gain for each channel was then calculated on a run-by-run basis, using the gains calculated from the most recent pedestal run, the temperature measurements, and the following formula:

$$G = G_0 + \frac{\mathrm{d}G}{\mathrm{d}T} T_{\mathrm{diff}}, \tag{7.1}$$

where G_0 is the gain of the preceding pedestal run, T_{diff} is the temperature difference between the current run and the preceding pedestal, and $\frac{\mathrm{d}G}{\mathrm{d}T}$ is the rate of change of gain with temperature, found to be $-0.67\times10^5/^\circ\mathrm{C}$. This removed much of the charge scale variation between runs.

As shown in figure 17, some residual temperature dependence is seen in the detector response after making the temperature-based correction, particularly in the period before regular pedestal runs were taken. A fit to the temperature data corresponding to the final five days in figure 17 indicates that the average temperatures were rising, resulting in the slight decrease in the Landau most probable values (MPVs) that is visible in the plot. To remove these variations, data from cosmic ray muons (collected coincidentally with beam events, in DAQ integration periods not associated with the beam) were processed from each run. The MPV of the charge distribution of

2013 JINST 8 P10019

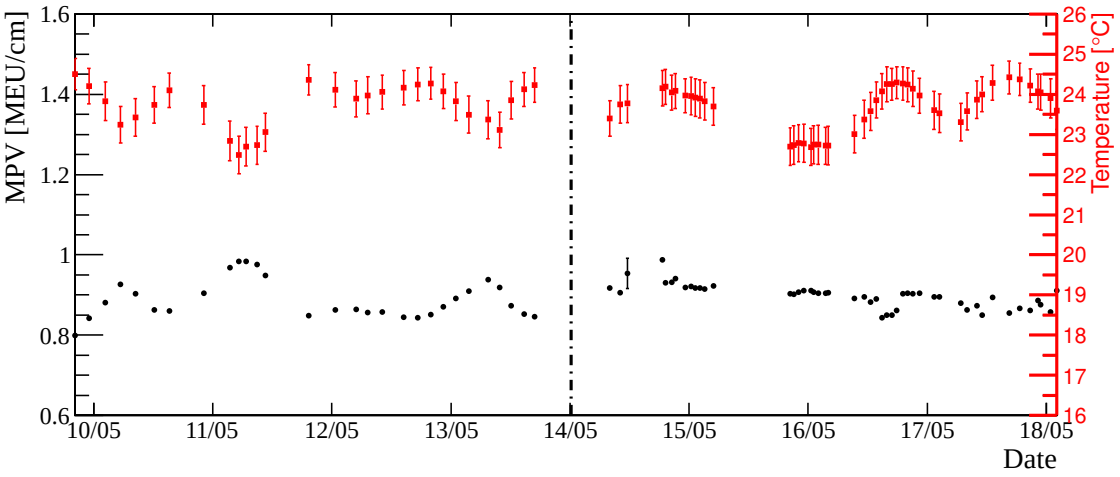

Figure 17. Time series of the average detector temperature and Landau most probable value (MPV) for muon hits in each run, after making a temperature-based gain correction. The dashed line represents the point at which pedestal runs began to be taken regularly.

single hits across all channels was then found for this sample, and used to scale hit charges for electron events in the run, equalizing the MIP scale for all data runs.

Monte Carlo samples for each individual testbeam run were produced using Geant4 [28]. A representation of the Ds-ECal geometry was constructed, and a monochromatic beam of electrons at each central beam momentum point was fired into the centre of the back-face of the Ds-ECal. The photosensor response was simulated utilizing data from test bench measurements and tuned using cosmic ray muon data, with special attention to simulating the temperature response of the photosensor. Monte Carlo samples were generated with temperatures identical to the average local temperature of each photosensor on a run-to-run basis. A similar cosmic ray muon sample was also generated at this temperature, and the calculated MPV was used to scale the electron hit charges.

In order to remove any poorly understood noise or readout-chip threshold variation, a charge threshold equivalent to 0.4 MIP units was implemented in the data and simulation. In addition, during the final processing of the data, any hits further than 8σ of the beam-time width from the peak cluster time were discarded to remove unsimulated cosmic events. The Monte Carlo data sets were then passed through the same calibration and reconstruction paths as data.

The procedure described successfully accounted for the average gain variation over the running period due to temperature variation. It was not, however, possible to account for sensor-to-sensor variations or temperature shifts within individual runs.

7.5 Testbeam performance

The testbeam data were used to calculate the performance of the Ds-ECal in the reconstruction of incident particles, particularly electrons. The performance results for electrons will be shown here.

Figure 18 shows the measured energy resolution for electrons striking the centre of the ECal face, as a function of energy. It can be seen that the data and Monte Carlo agree reasonably well, but the data resolution is somewhat worse over the whole energy range, and particularly at lower energies. This may be accounted for in part by the intrinsic momentum spread of the beam, which

2013 JINST 8 P10019

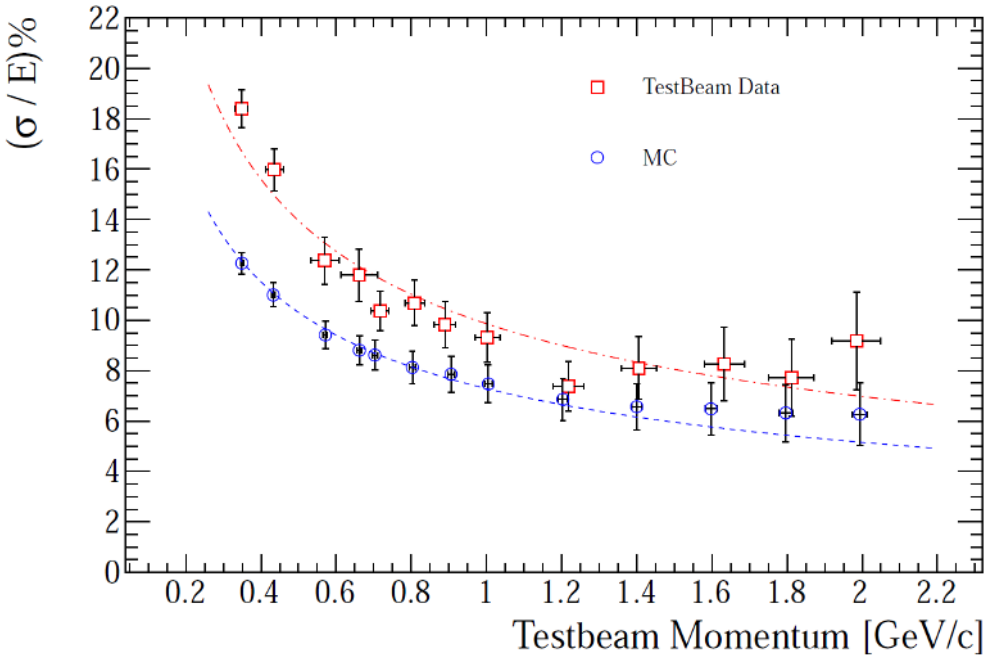

Figure 18. Measured energy resolution of the Ds-ECal for electromagnetic showers, for data and Monte Carlo. The dashed lines show a fit to a stochastic resolution model.

was not modelled in the Monte Carlo. In addition, the temperature-based gain corrections used for this data will only correct the mean photosensor gain across the Ds-ECal. A spread in MPPC gains due to temperature differences across the ECal is expected, but cannot be corrected because the temperatures of individual sensors could not be measured and were not modelled in the Monte Carlo, which assumes the same temperature for all sensors. This is expected to lead to a larger spread in measured particle energies.

Because of the limitations described above, the differences between data and Monte Carlo seen in figure 18 represent a worst-case scenario for the calculation of systematic uncertainties. Work is currently underway to replace this conservative estimate with one based on in-situ measurements.

Figure 19 shows the angular resolution of the Ds-ECal for normally incident electrons at a range of energies. Excellent agreement is seen between data and Monte Carlo over the full range of energies considered.

In summary, the T9 testbeam has provided useful information for the calculation of systematic uncertainties, and also gave an opportunity to test the detector and DAQ systems before they were integrated into the ND280. The data collected were also invaluable in the development of calibration and reconstruction code in advance of data from the full ND280 becoming available.

8 ECal commissioning and performance

8.1 Calibration

Precise calibration of ECal hits is vital for high-quality calorimetric performance. To this end, a set of procedures has been developed to calibrate out all significant instrumental effects, with the goal

2013 JINST 8 P10019

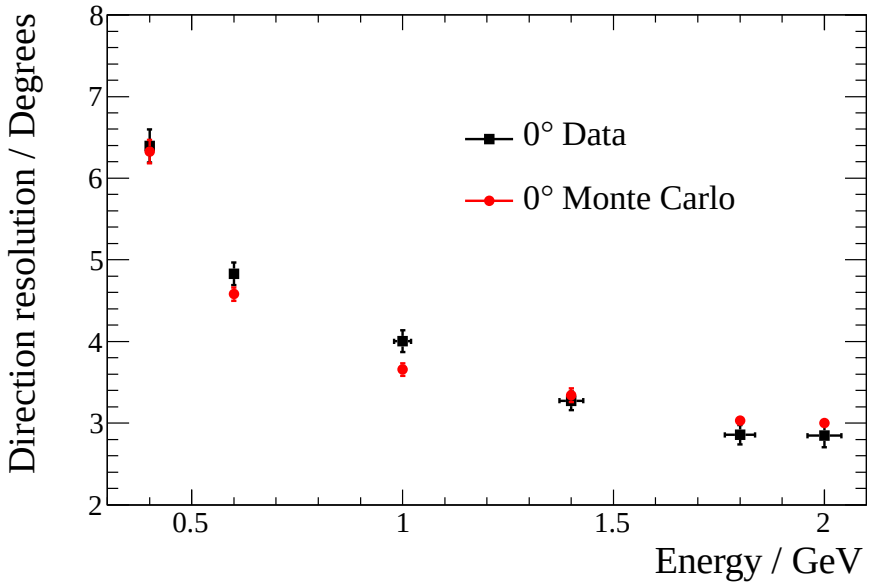

Figure 19. Angular resolution for electrons at normal incidence to the detector, in data and Monte Carlo, as a function of energy.

of obtaining the energy deposited in the scintillator giving rise to the hit, and the precise time at which the energy was deposited. The calibration can be separated into two main categories which are described below: energy calibration and timing calibration.

Energy calibration can be logically split into three steps — going backwards down the readout chain from the ADC value registered by the electronics to the anode charge from the MPPC, from this to the number of photons incident on the MPPC face, and from this to the energy deposit in the scintillator.

The first step involves subtracting the electronics pedestal from the ADC counts. This pedestal is the ADC value registered in the absence of any physics signal, and is different for each channel and readout cycle. Dedicated runs are taken once a week during beam down-times to measure the pedestals separately for each cycle, and a per-channel average over cycles is calculated every three hours from noise spectra recorded by the DAQ in normal running. The diurnal variation in pedestals, due to temperature changes at the electronics, is up to a few ADC counts, so fine-granularity corrections are important.

The next step is to convert the pedestal-subtracted ADC into an anode charge. The electronics response is not perfectly linear, and the calibration must also incorporate the transition from high gain to low gain ADC channels. Both the high gain and low gain response are mapped using the TFB's ability to inject a known charge onto each channel in turn. These charge injection curves are parametrized for both high and low gain channels using two cubic polynomials joined with a sigmoid function to smoothly transition between them. The parametrized charge injection curves also allow us to calibrate the low gain channel response to the high gain channel. The switchover between the two channels is made at approximately 460 ADC counts in the high gain channel, which typically corresponds to about 21 PEU. An example of the charge injection curves is shown

2013 JINST 8 P10019

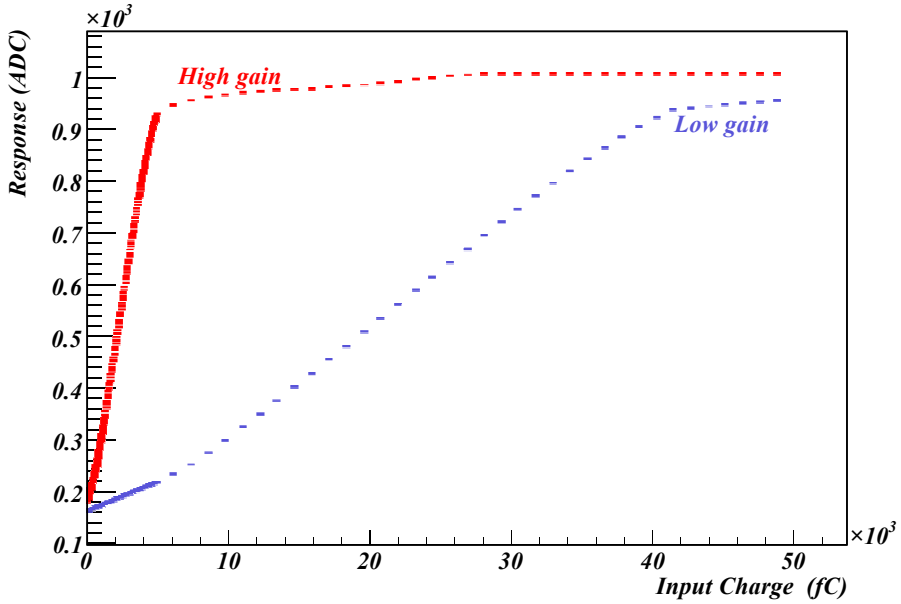

Figure 20. High and low gain ADC response of a typical Trip-T channel. Charge is injected using an onboard capacitor controlled by a Digital-to-Analogue Converter (DAC). The injected charge is calculated from the DAC setting. For comparison, a typical MIP deposits of order 10^7 electrons or 1.6×10^3 fC of charge.

in figure 20. A typical MIP deposits of order 10^7 electrons or 1.6×10^3 fC of charge, i.e. in the first bin on the plot. More information about the charge injection calibration is available in reference [29]. The parameters for this calibration are rather stable over time, so are only updated around once per running period.

To convert the calculated anode charge to an estimate for the number of photons incident on the MPPC, we first convert the charge into a number of PEU, by dividing by the gain of the MPPC. The gains for each channel are calculated for every three hours of data, using the same noise spectra as the pedestal drift, and fitting the position of the first non-pedestal peak in the noise spectrum which is due to a single pixel firing in the device. Again, diurnal temperature variations have non-negligible effects on the gain, so this granularity is required. We then need to convert this number of pixels to a number of photons. For low light levels, this conversion can be approximated by dividing by the PDE of the MPPC; however, it is complicated by saturation effects (the MPPC has a finite number of pixels and therefore a limited dynamic range), and also by after-pulsing and crosstalk, which cause the effective PDE to be larger than the true value.[2] The resulting response function cannot easily be calculated analytically, and is therefore modelled on testbench measurements. A single response function is used for every channel, but the parameters are in turn functions of the device gain, so that changes in PDE and other parameters with overvoltage can be taken into account.

Next, we need to convert the number of incident photons to an energy deposit. This needs to be done for each channel, as there will be some non-uniformity due to, for example, the differ-

[2] A detected photon has approximately a 10% probability of initiating a secondary avalanche; therefore, the number of avalanches is in general higher than the number of detected photons

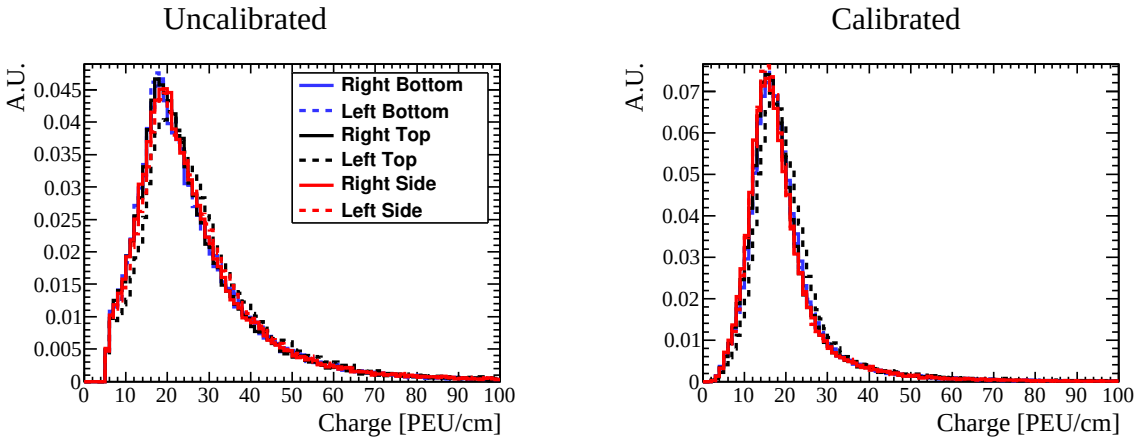

Figure 21. The effect of the attenuation and uniformity corrections on the hit charge distributions for through-going cosmic muons in the six modules of the barrel-ECal, shown by the six curves in each plot. The left side shows the distributions with the pedestal and gain corrected; the right side adds corrections for attenuation and differences caused by non-uniformity of scintillator bars and WLS fibres. Distributions shown here are summed within a module, but the corrections are applied on a per channel basis. The slight variation between modules is typical and insignificant.

ences between channels in the optical coupling between the fibre and the MPPC. The correction is done using empirical data, taking a sample of cosmic muon tracks passing through the ECal, performing all other calibrations, including attenuation in the fibre (described below), and track path-length through the scintillator bar. The corrected hit size distribution for each channel is fitted with a Landau distribution convolved with a Gaussian smearing. The effect of the attenuation and uniformity corrections is shown in figure 21; the distributions on the right side are used for the Landau-Gaussian fit. This is used to calculate the expected hit size for a MIP-size energy deposit at a fixed (1 m) distance from the sensor; the result is used as a divisor to equalize the sizes of hits between bars. The signal produced by this "ideal MIP" varies between modules and scintillator bar orientations, but to give a sense of scale, a muon passing approximately perpendicularly through the centre of the Ds-ECal typically leads to approximately 19 pixel avalanches at each sensor, corresponding to approximately 17 detected photons.

It is also necessary to correct for the attenuation of photons in the WLS fibres, which is significant over the length of the ECal bars. This calibration is done after the reconstruction has matched tracks between the two views of the ECal, so that the component of the hit position along the length of the scintillator bar can be estimated. The attenuation profile is modelled as a sum of two exponential functions, with an additional correction for the mirroring of the single-ended fibres. This correction is stable over time, and is calculated separately for each orientation of bar in each module using cosmic muon tracks. Figure 22 shows the time stability of the energy calibration over one period of beam running.

The timing calibration also involves several distinct steps. Each hit is time-stamped using the TFB clock, based on the time at which the channel's discriminator was triggered. The discriminator trigger is nominally set at a level of 3.5 PE. The TFB clocks lag the global detector clock from

2013 JINST 8 P10019

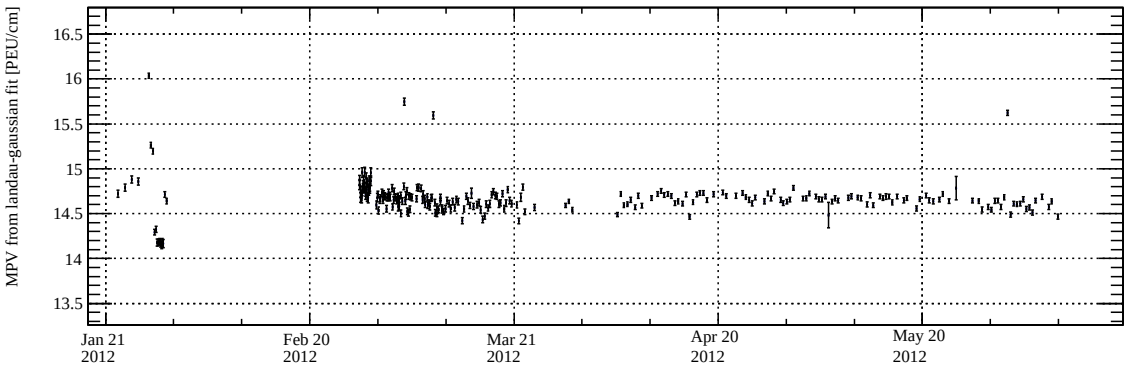

Figure 22. The muon MIP response as a function of time for a period of beam running.

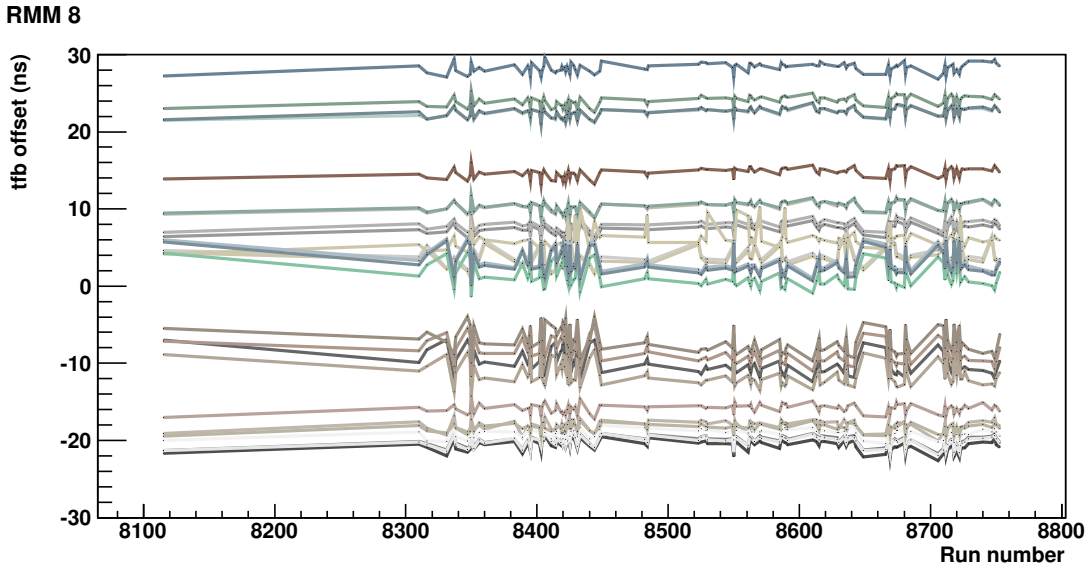

Figure 23. The TFB offset before correction for all channels on one RMM as a function of time for a period of beam running. Each line shows one TFB.

which they are synchronized, due to delays in the cabling and electronics used to distribute the clock signals. This effect will be different for each TFB depending on the cable lengths. The differences between TFBs within the ECal are calculated by considering cosmic muons that leave hits in channels corresponding to different TFBs, and correcting the hit times for fibre delay and the transit time of the muon. Synchronizing the ECal with the rest of the detector is achieved using a similar method. Figure 23 shows the offset for the TFBs on one RMM over a period of runs.

A 'timewalk' correction is also applied to the hit times. The decay that causes the WLS fluors to radiate occurs with a half life of a few nanoseconds, leading to the photons arriving at the MPPC face over a finite time period. The analogue electronics also have a finite rise time; both of these effects result in a delay between the idealized propagation of the signal and it crossing the discriminator threshold. These delays depend on the total hit charge and tend to a small constant

2013 JINST 8 P10019

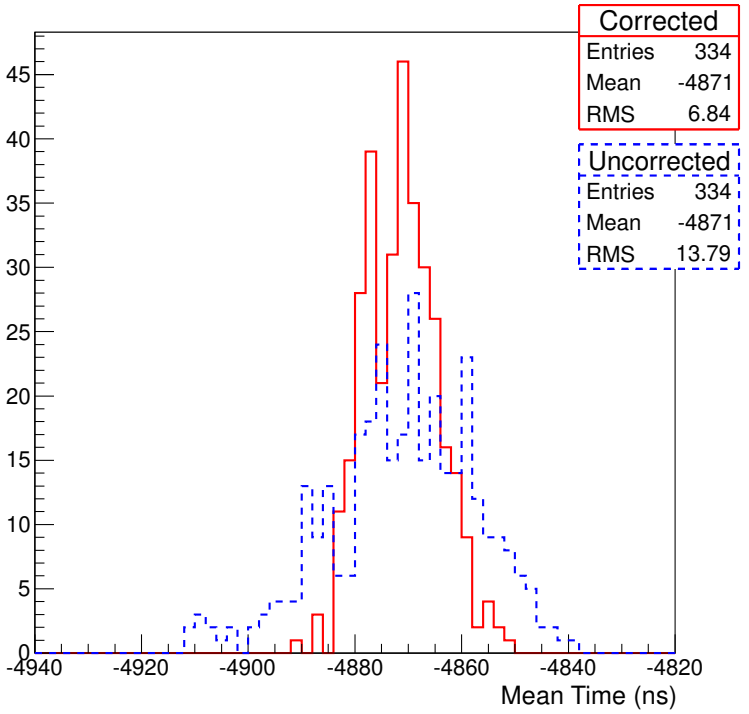

Figure 24. The distributions of mean hit time values for cosmic muons for each channel of the tracker-ECal (corresponding to 334 TFBs) before timing calibration (blue dashed line) and after timing calibration (red solid line).

offset for large hits. The optical component of the timewalk is a stochastic process and affects the timing resolution, but the average effect can be removed with an analytic function based on an exponential photon arrival time distribution, using the known decay time of the relevant state in the WLS fibre. Finally, the travel time for photons in the WLS fibre must be calibrated. This is done after the reconstruction has matched hits between views, so that the light travel distance is known.

Figure 24 shows a comparison between the mean hit time values of each TFB channel during cosmic muon triggers before and after corrections. The distribution of mean hit time values narrows by a factor of two in the RMS, and approaches the limit set by the trigger logic. The central value corresponds to the time delay between a cosmic muon being observed and the corresponding trigger being issued by the master clock. The 'ideal case' resolution for this delay is approximately 4 ns RMS, but it is dominated by the 10 ns granularity of MCM clock and the fluor decay time, both of which are non-Gaussian. Resolution on the time between two hits from a single muon is rather better, and the time resolution on the entire reconstructed ECal track is better still. The dominant uncertainty comes from the fluor, so each hit provides a largely-independent estimate. For a typical track or shower reconstructed in the ECal, the time resolution is approximately 1 ns or less, which is sufficient for direction discrimination when used in combination with information from other subdetectors.

2013 JINST 8 P10019

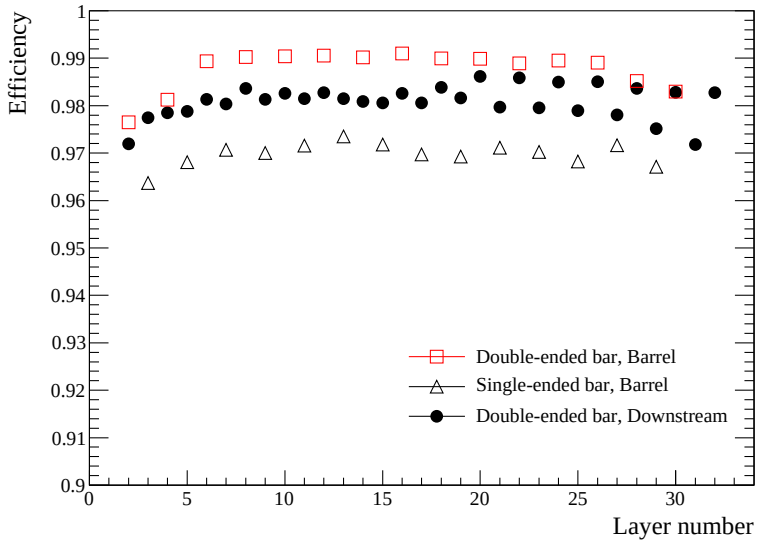

Figure 25. The hit efficiency by layer for bars in the Ds-ECal and barrel-ECal. Layer number increases from the central region to the exterior of the detector.

8.2 Hit efficiency

The hit efficiency for the ECal can be determined by looking at a sample of through-going cosmic muons; if the scintillator bars in layer $n+1$ and layer $n-1$ are hit, the cosmic ray should have passed through a scintillator bar in layer n. The sample of cosmic rays used for this measurement ensures that the cosmic rays are isolated from other activity in the ECal, resulting in an accurate measure of the layer-by-layer efficiency. The hit efficiencies by layer are shown in figure 25. The average layer efficiency in the Ds-ECal is 98.1% and the average layer efficiency in the barrel-ECal for double-ended bars is 98.8% and for single-ended bars is 97.0%. The lower efficiency in the single-ended bars is due to the reduced light collection from only one MPPC.

8.3 Time stability and beam position

The Ds-ECal was in operation at the ND280 site since November 2009, and the barrel-ECal since November 2010. Over that time period, the operation of the ECal has been stable. The stability of the operation can be observed from the interactions measured while the beam is on. A low-level selection requiring only the reconstruction of an energy cluster produces a sample of events occurring in the ECal. Note that this selection does not correspond to a physics selection, but simply allows for an accounting of activity in the ECal while the beam is on. Figure 26 shows the number of interactions in the ECal as a function of time, normalized to the number of protons on target (POT). The rate is steady over the run periods.

Since the ND280 detector operates off axis, the number of events as a function of spatial position is expected to be greater near to the axis of the beam and lesser away from the axis of the beam. The position of the beam centre in the coordinates of the ND280 is approximately (+3200, -9400) mm, below the lower right quadrant of figure 27, and as shown in the figure, the number of interactions near the beam is significantly greater than away from the beam. The beam spread is approximately 4.5 m as measured by the INGRID on-axis detector, and depends on neutrino energy.

2013 JINST 8 P10019

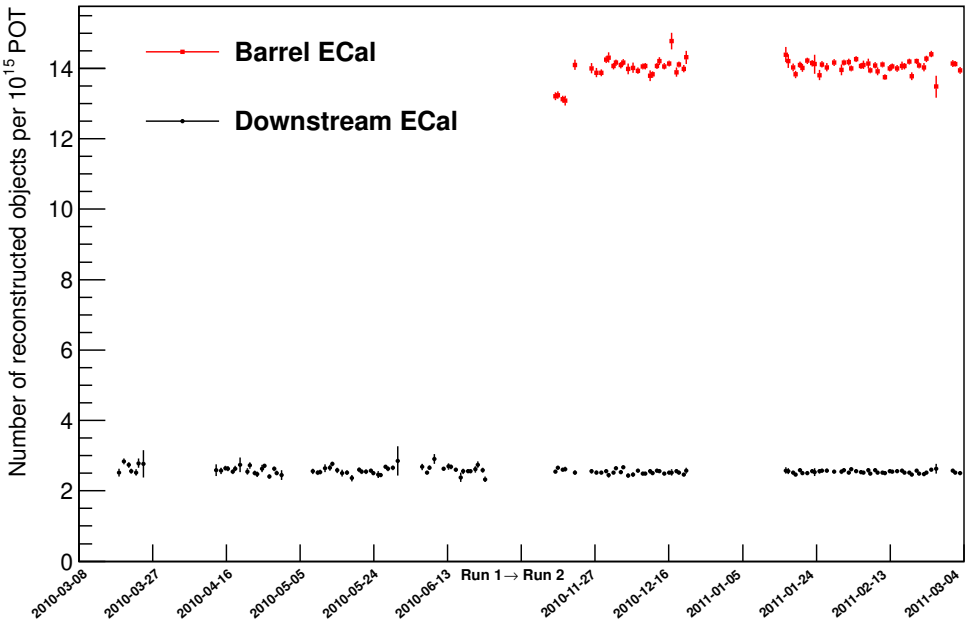

Figure 26. The rate of interactions in the ECal during beam operations over time for T2K Run 1 and Run 2. The black points (at ≈ 2) show the Ds-ECal and the red points (at ≈ 14) show the barrel-ECal. Note the gap marked on the time axis indicating the gap between Runs 1 and 2, when the barrel-ECal was installed.

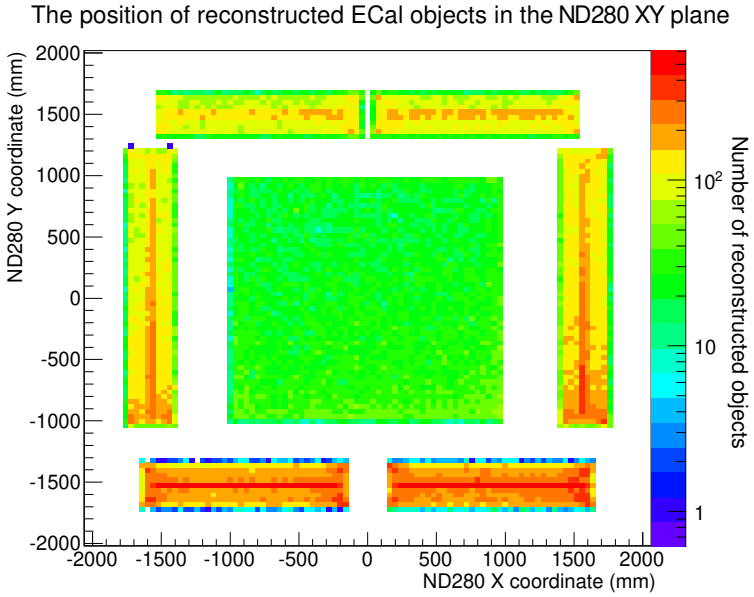

Figure 27. The charge weighted position of interactions reconstructed in the ECal. The position of the centre of the beam is to the lower right, and as a result, more events occur in the bottom right of the ECal than the top left. Events that are recorded in the centre of each module are through-going MIPs that leave approximately the same charge in each layer, and therefore have a charge weighted position in the centre.

2013 JINST 8 P10019

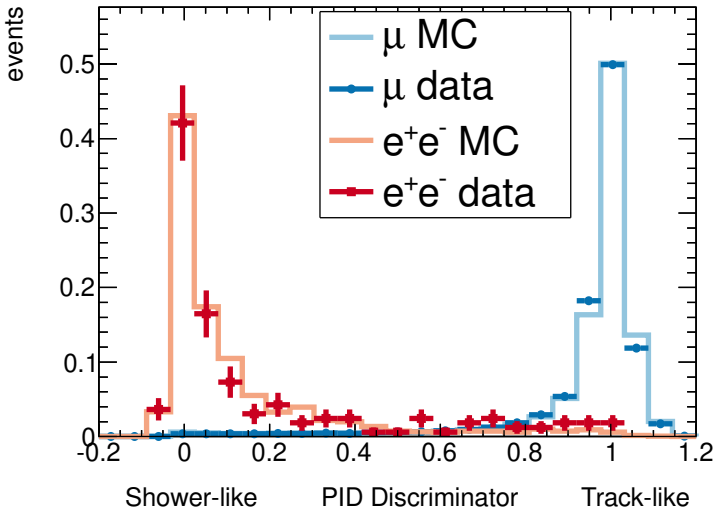

Figure 28. The discrimination between track-like (muon-like) and shower-like (electron-like) samples in the Ds-ECal. Solid lines show Monte Carlo information and points show data samples described in the text.

8.4 Particle identification

One of the goals of the ECal is to provide discrimination between electrons and muons in the region of phase space that is not covered by the particle identification from the tracker. The first method for particle identification constructed for the ECal was intended to maximize the separation of track-like (muon-like) and shower-like (electron-like) interactions. The discriminator is constructed as a neural network [30] using low level quantities from the reconstruction.

To test the discriminator, samples of muons and electrons are selected from the data. For the Ds-ECal (barrel-ECal), the muons selected are 'through-going' muons that have one track component in each of the three TPC modules and the Ds-ECal (barrel-ECal). Additionally, the track must appear 'muon-like' to the TPC [12]. The electron sample is produced by looking at photon pair production in the FGD [13], requiring tracks with opposite charge, at least one TPC component in the track, and that the TPC component appears 'electron-like'. Electrons or positrons that enter the tracker-ECal are added to the sample. In these control samples, the median muon momentum is 1.7 GeV/c, with muon momenta ranging from 300 MeV/c to 10 GeV/c; the median electron or positron momentum is 165 MeV/c. These energies are typical of events seen from the neutrino beam. Additionally, the discriminator is insensitive to the muon momentum provided that it is greater than approximately 300 MeV/c; that is, provided that the muon is MIP-like.

The electron and muon samples are shown with the calculated discriminator in figures 28 and 29 for the Ds-ECal and barrel-ECal, respectively. For both, there is good agreement between the data and the Monte Carlo, and good separation between the muon and electron samples; however, the separation is somewhat better in the Ds-ECal than in the barrel-ECal due to the different $p-\theta$ distributions seen in each. The barrel-ECal , because of its position within the ND280, sees, on average, lower momentum particles with a higher angle of incidence than the Ds-ECal. This combination of properties presents greater challenges for reconstruction and particle identification.

2013 JINST 8 P10019

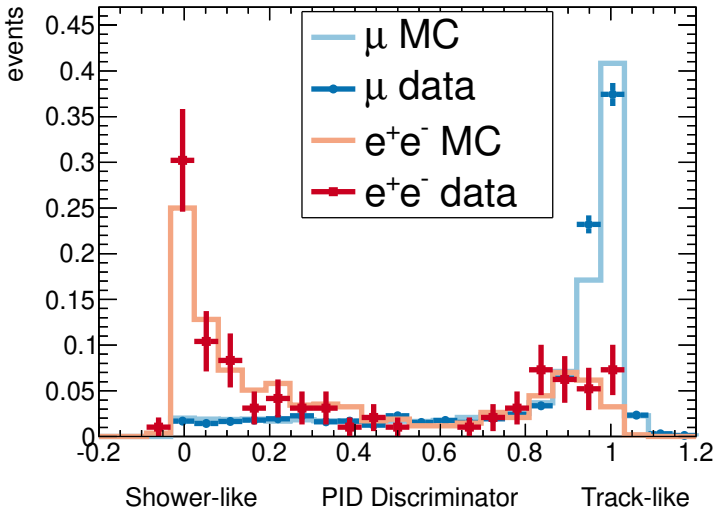

Figure 29. The discrimination between track-like (muon-like) and shower-like (electron-like) samples in the barrel-ECal. Solid lines show Monte Carlo information and points show data samples described in the text.

9 Summary

The electromagnetic calorimeter (ECal) for the T2K ND280 was designed and constructed in the U.K. during the period 2007-2010. The first module, the Ds-ECal, was tested in a charged-particle beam at CERN in spring 2009 and installed in the ND280 at J-PARC in time for the first T2K neutrino beam in January 2010. The testbeam data validated the design and operation of the system and have been used to characterize its response. The remaining 12 ECal modules were constructed in 2009-2010 and installed at J-PARC in time for the second neutrino data-taking period of T2K starting in fall 2010. The ECal has been operating stably and survived the great earthquake of March 2011 without any damage. The ECal has met its goals in terms of energy resolution and particle identification and is an integral part of the ND280. ECal data are used in the ND280 physics analyses and this is becoming more important as larger data samples are collected and more sophisticated analyses are being developed.

Acknowledgments

The ECal detector has been built and is operated using funds provided by the Science and Technology Facilities Council U.K. Important support was also provided by the collaborating institutions. Individual researchers have been supported by the Royal Society and the European Research Council. The authors also wish to thank CERN for support with the testbeam, FNAL for manufacturing the scintillator bars and preparing the wavelength-shifting fibres, and finally our T2K colleagues for their invaluable help during installation and commissioning of the detector.

2013 JINST 8 P10019

References

[1] K. Abe et al., *Measurements of the T2K neutrino beam properties using the INGRID on-axis near detector*, *Nucl. Instrum. Meth.* **A 694** (2012) 211 [arXiv:1111.3119].

[2] T2K collaboration, K. Abe et al., *The T2K Experiment*, *Nucl. Instrum. Meth.* **A 659** (2011) 106 [arXiv:1106.1238].

[3] SUPER-KAMIOKANDE collaboration, Y. Fukuda et al., *The Super-Kamiokande detector*, *Nucl. Instrum. Meth.* **A 501** (2003) 418.

[4] MINOS collaboration, P. Adamson et al., *Measurement of Neutrino and Antineutrino Oscillations Using Beam and Atmospheric Data in MINOS*, *Phys. Rev. Lett.* **110** (2013) 251801 [arXiv:1304.6335].

[5] K2K collaboration, M. Ahn et al., *Measurement of Neutrino Oscillation by the K2K Experiment*, *Phys. Rev.* **D 74** (2006) 072003 [hep-ex/0606032].

[6] T2K collaboration, K. Abe et al., *Evidence of Electron Neutrino Appearance in a Muon Neutrino Beam*, *Phys. Rev.* **D 88** (2013) 032002 [arXiv:1304.0841].

[7] T2K collaboration, K. Abe et al., *First Muon-Neutrino Disappearance Study with an Off-Axis Beam*, *Phys. Rev.* **D 85** (2012) 031103 [arXiv:1201.1386].

[8] DAYA-BAY collaboration, F. An et al., *Observation of electron-antineutrino disappearance at Daya Bay*, *Phys. Rev. Lett.* **108** (2012) 171803 [arXiv:1203.1669].

[9] RENO collaboration, J. Ahn et al., *Observation of Reactor Electron Antineutrino Disappearance in the RENO Experiment*, *Phys. Rev. Lett.* **108** (2012) 191802 [arXiv:1204.0626].

[10] T2K collaboration, K. Abe et al., *Indication of Electron Neutrino Appearance from an Accelerator-produced Off-axis Muon Neutrino Beam*, *Phys. Rev. Lett.* **107** (2011) 041801 [arXiv:1106.2822].

[11] S. Assylbekov, G. Barr, B. Berger, H. Berns, D. Beznosko et al., *The T2K ND280 Off-Axis Pi-Zero Detector*, *Nucl. Instrum. Meth.* **A 686** (2012) 48 [arXiv:1111.5030].

[12] T2K ND280 TPC collaboration, N. Abgrall et al., *Time Projection Chambers for the T2K Near Detectors*, *Nucl. Instrum. Meth.* **A 637** (2011) 25 [arXiv:1012.0865].

[13] T2K ND280 FGD collaboration, P. Amaudruz et al., *The T2K Fine-Grained Detectors*, *Nucl. Instrum. Meth.* **A 696** (2012) 1 [arXiv:1204.3666].

[14] T2K ND280 SMRD collaboration, S. Aoki et al., *The T2K Side Muon Range Detector*, *Nucl. Instrum. Meth.* **A 698** (2013) 135 [arXiv:1206.3553].

[15] B. Still, *T2K ND280 Pi0 electromagnetic calorimeter*, Ph.D. thesis, University of Sheffield, U.K. (2010) [http://www.t2k.org/docs/thesis/004].

[16] A. Vacheret et al., *Characterization and Simulation of the Response of Multi Pixel Photon Counters to Low Light Levels*, *Nucl. Instrum. Meth.* **A 656** (2011) 69 [arXiv:1101.1996].

[17] MINOS collaboration, D. Michael et al., *The Magnetized steel and scintillator calorimeters of the MINOS experiment*, *Nucl. Instrum. Meth.* **A 596** (2008) 190 [arXiv:0805.3170].

[18] G. Davies, *Understanding and calibrating the DS-ECal for T2K's ND280*, Ph.D. thesis, University of Lancaster, U.K. (2011) [http://www.t2k.org/docs/thesis/009].

[19] P. Border et al., *A large liquid scintillator detector for a long baseline neutrino oscillation experiment*, *Nucl. Instrum. Meth.* **A 463** (2001) 194.

2013 JINST 8 P10019

[20] M. Yokoyama et al., *Application of Hamamatsu MPPC to T2K Neutrino Detectors*, Nucl. Instrum. Meth. **A 610** (2009) 128 [arXiv:0807.3145].

[21] Hamamatsu Photonics K.K., Solid State Division, *Hamamatsu MPPC (multi-pixel photon counter S10362-11 series*, http://www.hamamatsu.com/resources/pdf/ssd/s10362-11_series_kapd1022e06.pdf

[22] M. Ward, *Multi-Pixel Photon Counter characterisation for the T2K near detector electromagnetic calorimeter*, Ph.D. thesis, University of Sheffield, U.K. (2009) [http://www.t2k.org/docs/thesis/032].

[23] M. Yokoyama et al., *Performance of Multi-Pixel Photon Counters for the T2K near detectors*, Nucl. Instrum. Meth. **A 622** (2010) 567 [arXiv:1007.2712].

[24] M. Haigh, *Beam extrapolation and photosensor testing for the T2K experiment*, Ph.D. thesis, University of Warwick, U.K. (2011) [http://www.t2k.org/docs/thesis/006].

[25] A. Vacheret et al. *The front end readout system for the T2K-ND280 detectors*, *IEEE Nucl. Sci. Conf. R.* **3** (2007) 1984.

[26] S. Ritt, P. Armaudruz and K. Olchanski, *MIDAS (Maximum Integration Data Acquisition System)*, https://midas.psi.ch.

[27] G. Ward, *A Calibration System for the T2K ND280 Electromagnetic Calorimeters*, Ph.D. thesis, University of Sheffield, U.K. (2010), [http://www.t2k.org/docs/thesis/033].

[28] GEANT4 collaboration, S. Agostinelli et al., *GEANT4: a Simulation toolkit*, Nucl. Instrum. Meth. **A 506** (2003) 250.

[29] A. Waldron, *Neutrino oscillation parameters from ν_e appearance in the T2K experiment*, Ph.D. thesis, University of Oxford, U.K. (2012) [http://www.t2k.org/docs/thesis/037].

[30] C.M. Bishop, *Neural networks for pattern recognition*, Clarendon Press, Oxford, U.K. (1995).

2013 JINST 8 P10019